CHEMICAL NONEQUILIBRIUM EFFECTS ON THE FLOW IN THE WINDWARD PLANE OF SYMMETRY OF A BLUNTED DELTA ORBITER

by

J. A. Lordi and R. J. Vidal

Cornell Aeronautical Laboratory, Inc., Buffalo, New York

C. B. Johnson

NASA Langley Research Center, Hampton, Virginia

INTRODUCTION

The entry trajectory of the shuttle orbiter is designed for rapid deceleration of the vehicle at high altitude. The resulting combination of low velocity at high altitude leads to significant departures from chemical equilibrium in the flow field for that portion of the flight where real gas effects are important. In this paper, the extent, and some of the consequences, of nonequilibrium effects in the inviscid orbiter flow field are examined. To this end, calculations have been made for the reacting flow along selected streamlines in the windward plane of symmetry of a blunted delta shape representative of a shuttle orbiter.

An approximate model of the pressure field in the windward plane of symmetry of a blunted delta wing was constructed from wind tunnel measurements of the body surface pressure distribution and approximate calculations of the shock shape and streamline locations. Then numerical solutions for the flow along streamlines were obtained for this pressure distribution. Solutions were obtained for both equilibrium and finite-reaction-rate, nonequilibrium chemical reactions. Since the streamtube solutions are much easier to compute than fully three-dimensional, reacting flows, results were obtained for a wide range of conditions. The validity of this approach is based on the assumptions that the pressure field is insensitive to nonequilibrium effects and that the flow along streamlines is quasi-one dimensional. Numerical solutions have been used to verify this approach for other blunted slender shapes such as spherically blunted cones.[1]

The experimental surface pressure distributions were obtained in the NASA Langley Research Center Mach 8 Variable-Density Tunnel.[2] Pressure data were obtained for two shuttle test shapes, a blunted delta and a straight body, at angles of attack of 0, 20°, 40°, and 60°. All of these experimental results are presented even though the reacting flow calculations were confined to angles of attack of 20° and 40°. The streamline flow calculations were obtained with a computer program[3] previously developed at the Cornell Aeronautical Laboratory for the quasi-one-dimensional, reacting flow of a general gas mixture. In the present work,* air was assumed to be composed of a neutral species N_2, O_2, NO, N, O and Ar. Ionization of NO was also included. The thermodynamic and chemical kinetic data employed in the calculations are listed in Ref. 3.

The present paper first presents the data for the body surface pressure distributions. Next the construction of the approximate model of the pressure field in the windward plane of symmetry is described. Then results of both equilibrium and nonequilibrium flow calculations are discussed for three typical shuttle trajectory points in the altitude range of 60.96 to 76.20 km (200,000 to 250,000 ft). Calculations are compared for two angles of attack, 20° and 40°, and two nose radii, 0.305 m (1 ft) and 1.22 m (4 ft). Finally, the implications of the departures from chemical equilibrium to shuttle technology are discussed. The questions of surface heating rates, boundary layer transition, and entropy layer swallowing are treated.

*The nonequilibrium flow studies were supported by the NASA Langley Research Center under Contract No. NAS 1-10710.

PRESSURE TEST MODELS
(Fig. 1)

A series of experiments to measure the windward surface pressure distributions on two shuttle orbiter test shapes were conducted in the NASA Langley Mach 8 variable-density hypersonic tunnel. Surface pressures were obtained for the blunted delta and straight bodies shown below.

DELTA-WING AND STRAIGHT-BODY MODELS FOR WIND TUNNEL PRESSURE MEASUREMENTS

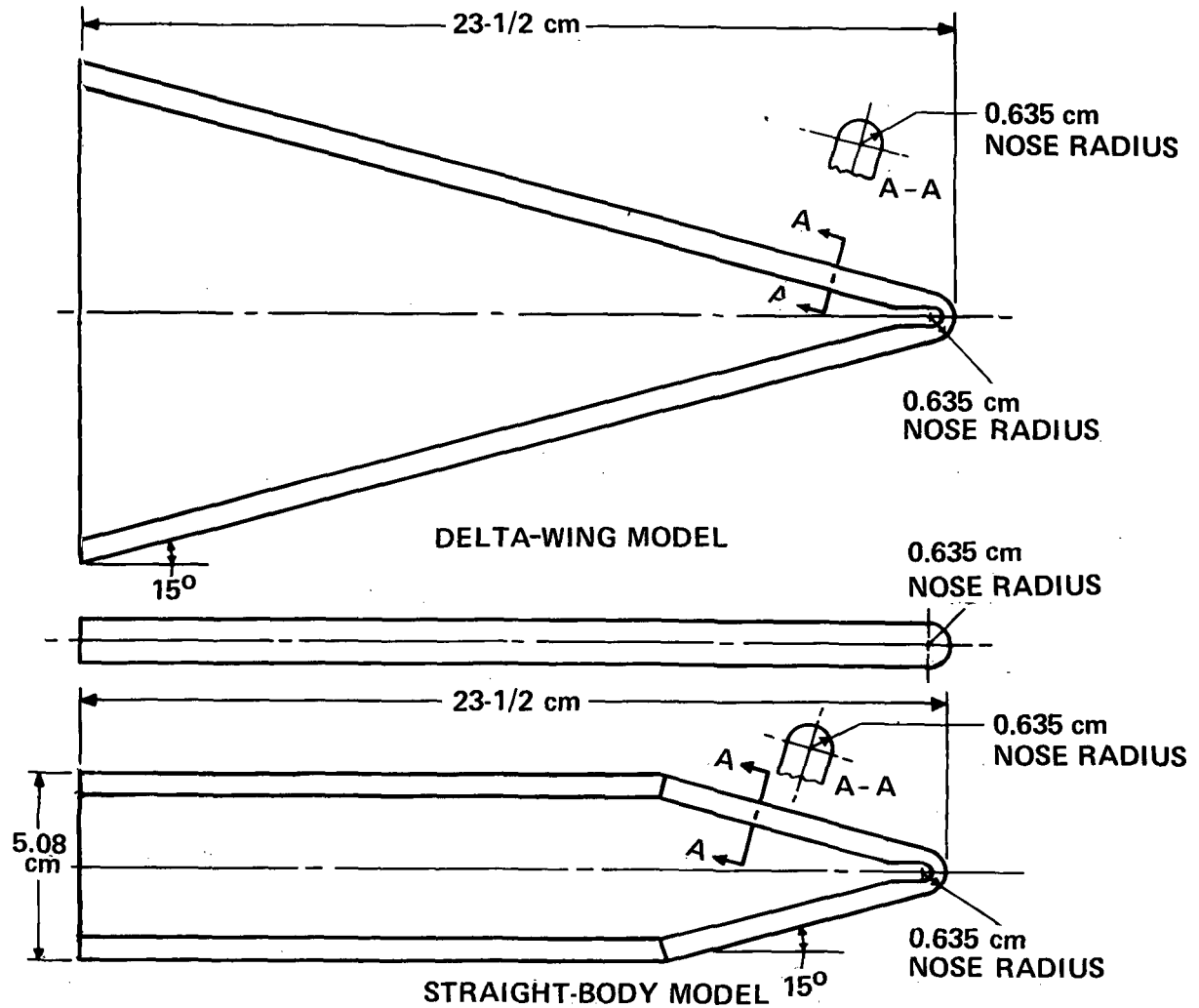

Figure 1

TEST CONDITIONS FOR PRESSURE MEASUREMENTS
(Fig. 2)

The tests were conducted at a nominal test-section Mach number of 8.0, unit Reynolds numbers in the range 8.8×10^6 m^{-1} to 41.5×10^6 m^{-1}, and angles of attack of 0^o, 20^o, 40^o, and 60^o. The Reynolds numbers given in the figure are based on model length.

EXPERIMENTAL TEST CONDITIONS

RUN NO.	MACH NO.	REYNOLDS NO.	ANGLE OF ATTACK	T_o	p_o
		x 10^{-6}	(deg)	(^oR)	(atm)
3	8.04	4.66	20	1455	102.7
4	7.99	3.37	20	1405	69.0
5	8.04	5.05	40	1405	105.1
6	7.99	3.37	40	1405	69.0
10	8.04	5.04	60	1385	102.4
11	7.99	3.41	60	1395	69.0
12	7.91	2.06	60	1305	36.4
28	8.11	8.46	0	1460	191
29	8.03	5.19	0	1315	96.3
30	8.03	4.53	20	1410	96.3
31	8.11	8.97	20	1410	191
32	8.03	4.64	40	1405	96.3
33	8.00	9.67	40	1380	193
34	7.95	2.32	60	1400	47.6
35	8.04	4.89	60	1385	95.2
36	8.00	9.75	60	1370	192

Figure 2

PRESSURE DATA FOR STRAIGHT BODY
(Fig. 3)

In this figure, the data from the experiments on the straight-wing body are tabulated. The data are given in the form p/p_{T_2} where p_{T_2} is the model stagnation pressure. The streamwise distance, S/R_N, is measured from the model centerline, b is the local span.

CENTERLINE PRESSURE DATA FOR THE STRAIGHT BODY

RUN NO.	28	29	30	31	32	33	34	35	36
S/R_N	p/p_{T_2}	p/p_{T_2}	p/p_{T_2}	p/p_{T_2}	p/p_{T_2}	p/p_{T_2}	p/p_{T_2}	p/p_{T_2}	p/p_{T_2}
1.134	.1918	.1948	.5421	.5480	.8874	.8439	.9525	.9766	.9570
1.571	.0466	.0449	.1969	.2002	.5270	.5104	.8587	.8963	.8802
2.071	.0344	.0337	.1491	.1537	.4870	.4724	.8233	.8635	.8465
2.823	.0302	.0305	.1331	.1357	.5110	.4983	.8187	.8573	.8386
4.114	.0236	.0273	.1275	.1311	.5262	.5218	.8249	.8573	.8374
5.614	.0194	.0225	.1315	.1382	.5230	.5053	.8203	.8589	.8276
7.611	.0152	.0178	.1491	.1546	.5222	.4995	.8295	.8565	.8284
10.61	.0152	.0194	.1602	.1663	.5374	.5143	.8387	.8698	.8296
13.61	.0143	.0202	.1602	.1608	.5350	.5088	.8233	.8526	.8096
16.06	.0152	.0225	.1578	.1562	.5278	.4979	.8157	.8378	.7943
20.61	.0131	.0187	.1501	.1560	.5194	.4892	.7839	.8182	.7727
24.06	.0144	.0211	.1598	.1593	.4749	.4318	.7667	.8009	.7473
28.61	.0118	.0163	.1477	.1458	.4806	.4398	.7527	.7867	.7361
32.61	.0144	.0195	.1412	.1382	.4312	.4034	.7418	.7772	.7298

Figure 3(a)

SPANWISE PRESSURE DATA FOR THE STRAIGHT BODY

	RUN NO.	28	29	30	31	32	33	34	35	36
S/R_N	2y/b	p/p_{T_2}	p/p_{T_2}	p/p_{T_2}	p/p_{T_2}	p/p_{T_2}	p/p_{T_2}	p/p_{T_2}	p/p_{T_2}	p/p_{T_2}
7.611	−.451	.0139	.0178	.1514	.1579	.5118	.4908	.8110	.8401	.8127
	−.180	.0139	.0194	.1491	.1529	.5214	.5018	.8249	.8542	.8269
	0	.0152	.0178	.1491	.1546	.5222	.4995	.8295	.8565	.8284
	.180	.0160	.0202	.1498	.1537	.5190	.5002	.8233	.8542	.8261
	.451	.0139	.0194	.1530	.1575	.5086	.4944	.8095	.8386	.8088
13.61	−.625	.0114	.0154	.1706	.1709	.5246	.5018	.7834	.8027	.7618
	−.438	.0118	.0170	.1658	.1663	.5334	.5135	.8064	.8355	.7931
	−.250	.0123	.0178	.1618	.1629	.5358	.5112	.8157	.8409	.8026
	−.125	.0148	.0194	.1594	.1604	.5350	.5092	.8249	.8511	.8088
	0	.0143	.0202	.1602	.1608	.5350	.5088	.8233	.8526	.8096
	.125	.0160	.0217	.1634	.1608	.5318	.5073	.8310	.8518	.8080
	.250	.0135	.0202	.1610	.1613	.5326	.5057	.8203	.8448	.8022
	.438	.0135	.0217	.1682	.1633	.5318	.5061	.8110	.8355	.7916
	.625	.0135	.0225	.1762	.1726	.5286	.5041	.7803	.8019	.7575
20.61	−.625	.0097	.0082	.1429	.1454	.4644	.4327	.7325	.7685	.7326
	−.438	.0135	.0163	.1534	.1551	.4935	.4608	.7714	.8024	.7548
	−.250	.0131	.0171	.1534	.1572	.5065	.4727	.7761	.8127	.7691
	−.125	.0127	.0154	.1517	.1577	.5194	.4826	.7870	.8190	.7723
	0	.0131	.0187	.1501	.1560	.5194	.4842	.7839	.8182	.7727
	.125	.0127	.0203	.1517	.1564	.5186	.4834	.7870	.8182	.7719
	.250	.0135	.0171	.1542	.1572	.5089	.4735	.7792	.8111	.7671
	.438	.0148	.0179	.1566	.1589	.4968	.4600	.7730	.8064	.7604
	.625	.0118	.0187	.1501	.1509	.4612	.4287	.7356	.7724	.7294
32.61	−.625	.0148	.0187	.1299	.1293	.4094	.3903	.6936	.7219	.6798
	−.438	.0157	.0187	.1372	.1348	.4272	.4053	.7232	.7519	.7095
	−.250	.0148	.0203	.1388	.1382	.4320	.4073	.7403	.7709	.7250
	−.125	.0165	.0187	.1396	.1382	.4344	.4065	.7434	.7732	.7290
	0	.0144	.0195	.1412	.1382	.4312	.4034	.7418	.7772	.7298
	.125	.0144	.0195	.1404	.1386	.4288	.4006	.7418	.7748	.7286
	.250	.0152	.0195	.1380	.1365	.4247	.4002	.7403	.7724	.7238
	.438	.0161	.0195	.1380	.1339	.4231	.3974	.7278	.7582	.7087
	.625	.0169	.0171	.1324	.1288	.4053	.3816	.6936	.7203	.6754

Figure 3(b)

PRESSURE DATA FOR THE DELTA BODY
(Fig. 4)

In this figure, the data are tabulated for the experiments on the blunted delta wing. Again the data are normalized by the model stagnation pressure and the streamwise distance is measured from the model centerline.

CENTERLINE PRESSURE DATA FOR THE DELTA BODY

RUN NO.	3	4	5	6	10	11	12
S/R_N	p/p_{T_2}	p/p_{T_2}	p/p_{T_2}	p/p_{T_2}	p/p_{T_2}	p/p_{T_2}	p/p_{T_2}
1.134	.4243	.4558	.7932	.7845	.9745	.9761	.9540
1.571	.1710	.1882	.4849	.4720	.8886	.9367	.8570
2.071	.1355	.1459	.4620	.4438	.8651	.8494	.8314
2.823	.1243	.1347	.4944	.4691	.8593	.8466	.8314
4.114	.1184	.1347	.4963	.4832	.8475	.8466	.8264
5.614	.1262	.1431	.4868	.4889	.8475	.8382	.8161
7.611							
10.61	.1496	.1572	.4924	.4889	.8475	.8579	.8212
13.61	.1516	.1657	.4887	.4973	.8553	.8579	.8264
16.61	.1399	.1572	.4849	.4917	.8690	.8748	.8417
20.61	.1457	.1572	.5020	.5001	.8593	.8720	.8417
24.61	.1574	.1684	.4811	.4944	.8475	.8579	.8314
28.61	.1399	.1684	.5096	.5114	.8358	.8438	.8161
32.61	.1418	.1572	.4754	.4860	.8241	.8298	.8161

Figure 4(a)

SPANWISE PRESSURE DATA FOR THE DELTA BODY

	RUN NO.	3	4	5	6	10	11	12
S/R_N	2y/b	p/p_{T_2}	p/p_{T_2}	p/p_{T_2}	p/p_{T_2}	p/p_{T_2}	p/p_{T_2}	p/p_{T_2}
7.611	−.484	.1457	.1618	.4849	.4832	.8339	.8298	.8110
	−.193	.1360	.1516	.4868	.4748	.8514	.8466	.8212
	0	–	–	–	–	–	–	–
	.193	.1360	.1488	.4887	.4748	.8514	.8410	.8212
	.484	.1418	.1572	.4792	.4748	.8299	.8241	.8008
13.61	−.664	–	–	–	–	–	–	–
	−.483	.1554	.1684	.4868	.4944	.8397	.8438	.8161
	−.302	.1477	.1628	.4887	.4944	.8494	.8494	.8212
	−.121	.1516	.1657	.4887	.4973	.8534	.8607	.8264
	0	.1516	.1657	.4887	.4973	.8553	.8579	.8264
	.121	.1558	.1657	.4906	.4973	.8553	.8607	.8264
	.302	.1516	.1657	.4906	.4973	.8494	.8523	.8264
	.483	.1554	.1657	.4906	.4917	.8378	.8410	.8110
	.664	.1593	.1684	.4811	.4860	.8124	.8184	.7854
20.61	−.798	.1574	.1741	.4697	.4804	.7928	.7847	.7651
	−.588	.1516	.1684	.4868	.4860	.8553	.8579	.8212
	−.378	.1477	.1628	.4982	.4944	.8612	.8720	.8366
	−.210	.1477	.1600	.5001	.4973	.8593	.8720	.8366
	−.084	.1457	.1572	.5020	.5001	.8593	.8720	.8366
	0	.1457	.1572	.5020	.5001	.8593	.8720	.8417
	.084	.1457	.1572	.5020	.5001	.8593	.8748	.8417
	.210	.1477	.1600	.4982	.5001	.8612	.8748	.8468
	.378	.1477	.1684	.4924	.4973	.8632	.8748	.8468
	.588	.1535	.1741	.4849	.4973	.8534	.8466	.8314
	.798	.1574	.1769	.4678	.4832	.7811	.7819	.7549
32.61	−.856	.1328	.1741	.4639	.4776	.7440	.7481	.7344
	−.635	.1516	.1657	.4792	.4944	.8045	.8101	.7906
	−.414	.1457	.1628	.4899	.5086	.8202	.8241	.8110
	−.249	.1457	.1628	.4811	.5029	.8221	.8269	.8161
	−.138	.1457	.1628	.4811	.4944	.8241	.8298	.8161
	−.055	.1418	.1572	.4754	.4860	.8241	.8258	.8161
	0	.1418	.1572	.4754	.4860	.8241	.8298	.8161
	.055	.1438	.1572	.4734	.4889	.8241	.8298	.8161
	.138	.1399	.1572	.4716	.4917	.8221	.8269	.8110
	.249	.1438	.1600	.4754	.5001	.8221	.8269	.8110
	.414	.1438	.1600	.4754	.5001	.8182	.8241	.8059
	.635	.1477	.1600	.4716	.4832	.8026	.8101	.7957
	.856	.1554	.1713	.4527	.4720	.7381	.7424	.7344

Figure 4(b)

SCHLIEREN PHOTOGRAPHS OF MODEL FLOW FIELDS
(Fig. 5)

In the series of experiments to measure surface pressure on the shuttle test shapes, Schlieren photographs were also taken. The photographs from two of the test conditions are shown in this figure. The cases illustrated are the blunted-delta and straight body at an angle of attack of 40°.

For the blunted delta wing the shock shapes over the windward surface are quite straight for $\alpha = 20°$ and $\alpha = 40°$. In the nonequilibrium flow calculations described later in the paper the flow downstream of the nose is assumed to be a uniform flow region and this assumption appears to be accurate.

The comparison of the two Schlieren photographs shown here indicates that the difference in the body shapes is reflected in the shock shape for this angle of attack. Both the Schlieren photographs and the pressure data indicate that the cross flow begins to affect the inviscid flow in the windward plane of symmetry at $\alpha = 40°$. At $\alpha = 60°$, the difference in the shock shapes is more pronounced. Also, the windward centerline pressure decays toward the base of the body; the pressure decreases more rapidly for the straight-body. At an angle of attack of 20° the shock shapes and windward centerline pressure distributions are nearly the same for these two body shapes.

SCHLIEREN PHOTOGRAPHS OF MODEL FLOW FIELDS

$M_\infty = 8, \alpha = 40^o$

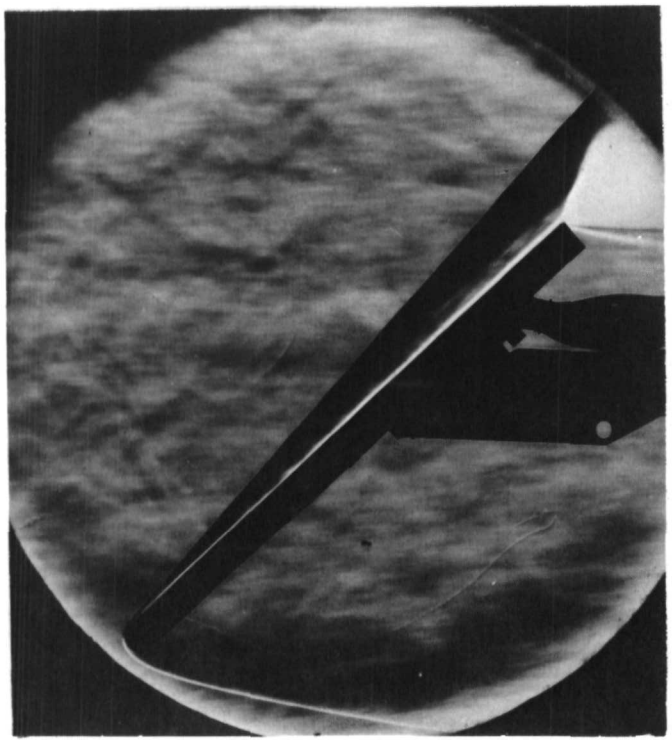

RUN 5

BLUNTED-DELTA BODY

RUN 33

STRAIGHT-BODY

Figure 5

WINDWARD SIDE CENTERLINE PRESSURE DISTRIBUTIONS FOR BLUNTED-DELTA SHAPE (Figs. 6 and 7)

In a previous study[1] of the hypersonic flow over blunted slender cones the surface pressure distribution was found to be insensitive to nonequilibrium effects. Since the flow along the windward plane of symmetry of the blunted-delta wing should be much like a cone flow this result has been used in the present study to scale the measured pressure distributions to flight conditions. The data were normalized by the tunnel-model stagnation pressure and the pressures on the flight vehicle were obtained by using the appropriate value of the stagnation pressure. The initial portion of the pressure distribution, i.e. between the stagnation point and the first data point, was taken from a composite correlation[1] of ideal gas, equilibrium and nonequilibrium flow calculations, and experimental data for the flow over spherically blunted bodies. The stagnation point was assumed to be the point where the body surface is normal to the free stream direction. A full scale body length of 45.6 m (150 ft) was used.

The body surface pressure distributions which were used in the streamtube calculations for $\alpha = 20°$ and $\alpha = 40°$ are shown in the next two figures, together with the experimental data on which they are based. Here and throughout the remainder of the paper S_b denotes distance along the surface streamline, measured from the stagnation point.

PRESSURE DISTRIBUTION ALONG WINDWARD CENTERLINE FOR BLUNTED-DELTA BODY, $\alpha = 20^{o}$

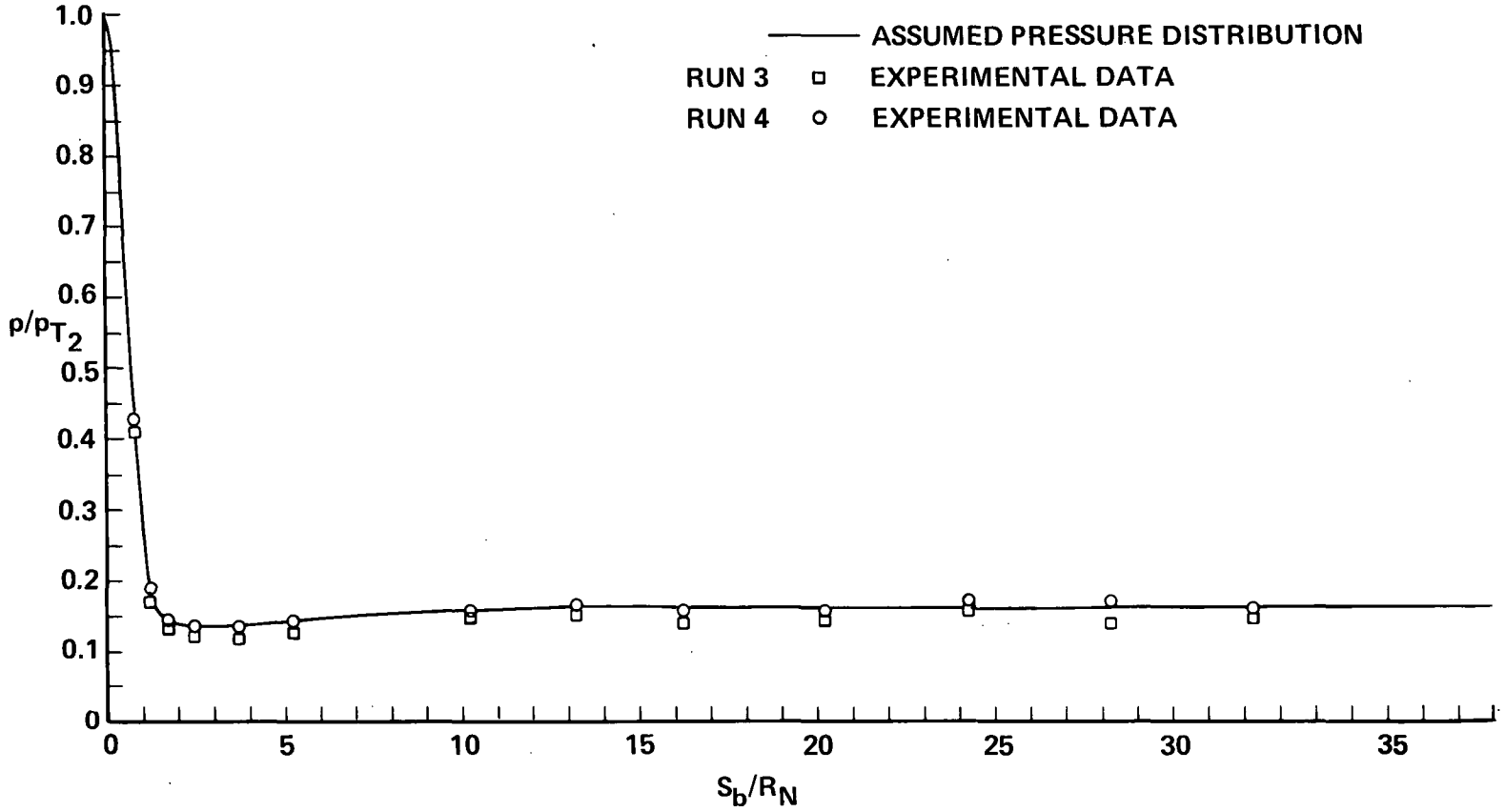

Figure 6

Page intentionally left blank

PRESSURE DISTRIBUTION ALONG WINDWARD CENTERLINE FOR BLUNTED-DELTA BODY, $\alpha = 40^{o}$

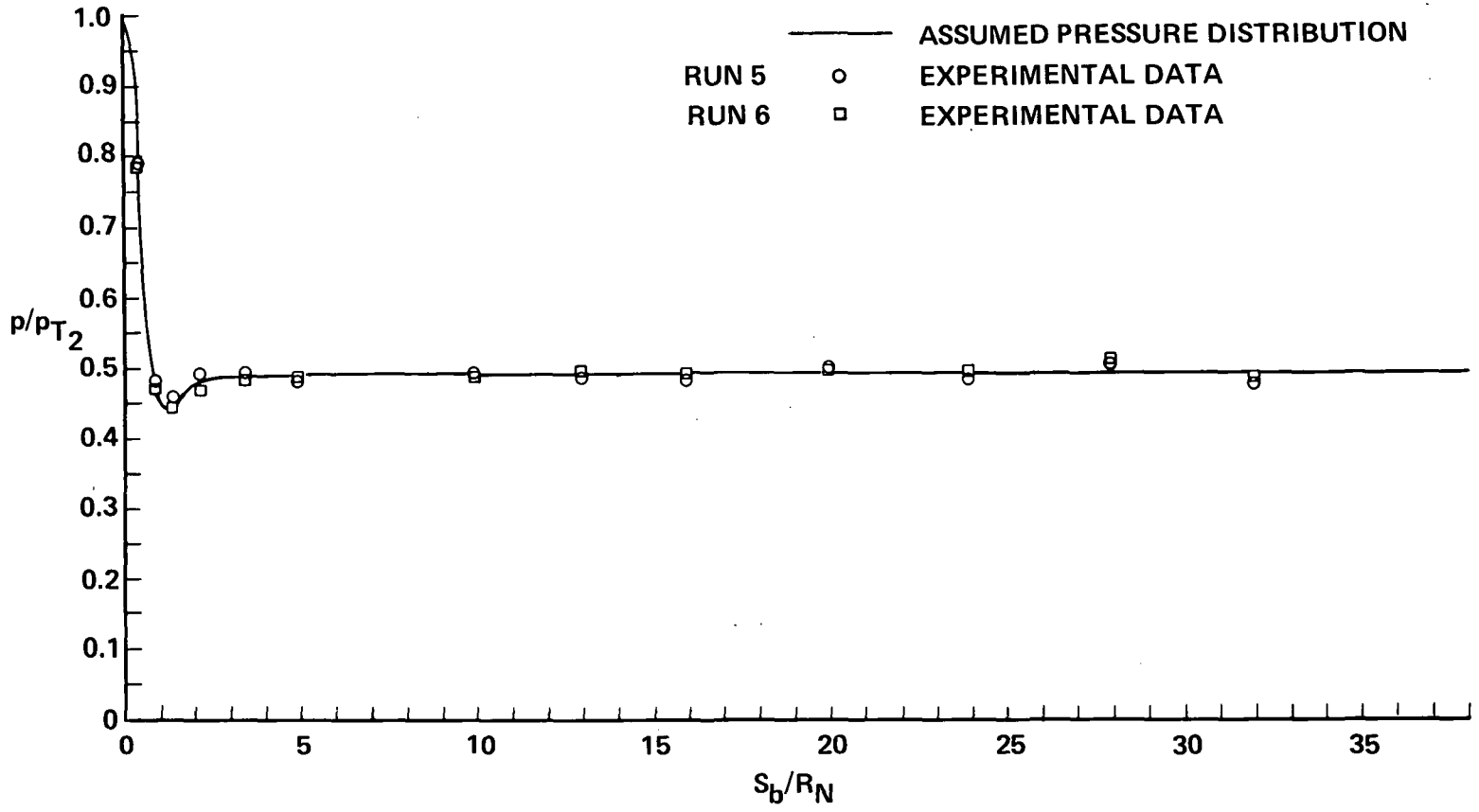

Figure 7

APPROXIMATE CALCULATION FOR SHOCK SHAPES AND STREAMLINE LOCATIONS (Figs. 8 and 9)

In order to obtain the pressure histories along streamlines off the body surface, an approximate model of the pressure field was devised. The shock shapes and streamline locations were obtained for equilibrium flow and again an appeal was made to the results for the flow about blunted cones. These results indicate that the shock shape as well as the surface pressure is insensitive to nonequilibrium effects.

The bow shock wave was assumed to be circular in the nose region and straight on the afterbody. The final shock angle was determined from the asymptotic, experimental surface pressure and oblique shock solutions for equilibrium flow. The circular portion of the shock was not taken to be concentric with the body. Rather, the center and radius of curvature were found by using a correlation for shock standoff distance at the stagnation point[4] and a mass balance to get the shock standoff distance at the body shoulder. The mass balance was done by assuming the flow in the stagnation region of the windward plane of symmetry to be the same as that in the axisymmetric flow over a blunted cone. The circular portion of the shock was joined to the straight portion at the point of tangency. In the nose region, the streamline locations also were found using a mass balance technique. The mass flux was assumed to vary linearly from the shock to the body along normals to the body surface. The solution for the equilibrium flow along the body streamline was computed using the known pressure distribution and an isentropic expansion from the known stagnation conditions. The values at the shock were obtained from the shock angle and shock tables for equilibrium flow.[5] In the afterbody region the streamlines were assumed to be parallel to the body. This assumption of a uniform pressure field on the afterbody appears justified both by Schlieren photographs obtained in this study (see Fig. 5) and three-dimensional flow calculations for equilibrium flow over a blunted delta wing.[6] Having established the streamline locations, the pressure distributions along them were computed assuming a linear variation between the pressure at the body and the shock, along normals to the body.

The shock shapes and streamline locations obtained for $\alpha = 20°$ and $\alpha = 40°$ are illustrated in the accompanying figures. The flow field consists basically of two regions: those streamlines which are processed by the strong curved shock and those which pass through the limiting oblique shock. The streamline which passes through the point where the shock becomes straight is referred to as the outer streamline or oblique-shock streamline. The pressure field between this streamline and the shock is assumed to be uniform. While these streamline locations may not be precise, the important point is that the pressure histories are realistic and the streamline calculations provide an accurate assessment of the nonequilibrium flow effects. Furthermore, for the extreme cases of the body surface streamline and the outer streamline, the calculations are good approximations to the results obtained from more general flow field calculations.

SHOCK SHAPE AND STREAMLINE PATTERN IN NOSE REGION, $\alpha = 20^{o}$

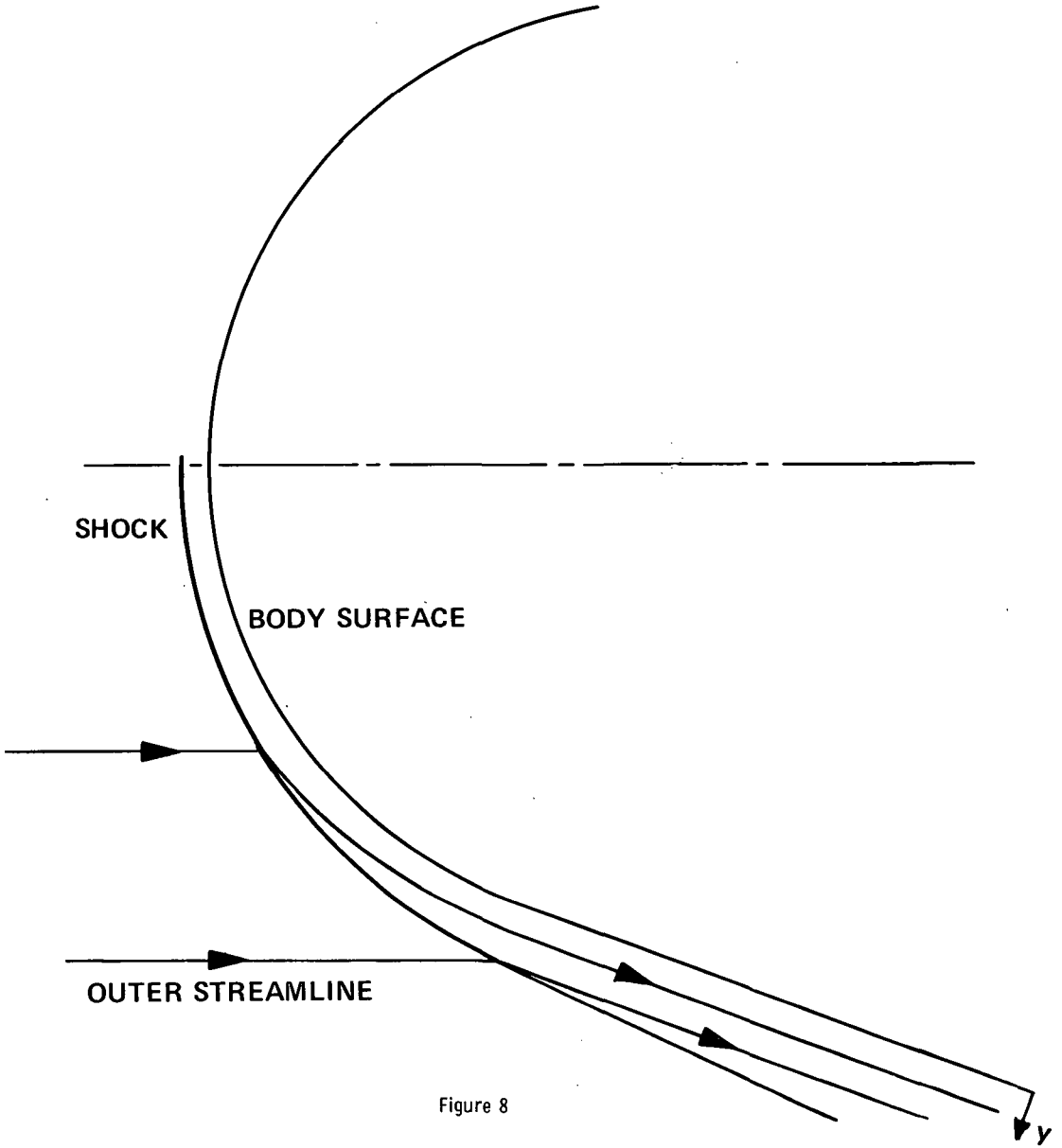

Figure 8

Page intentionally left blank

SHOCK SHAPE AND STREAMLINE PATTERN IN NOSE REGION $\alpha = 40^{o}$

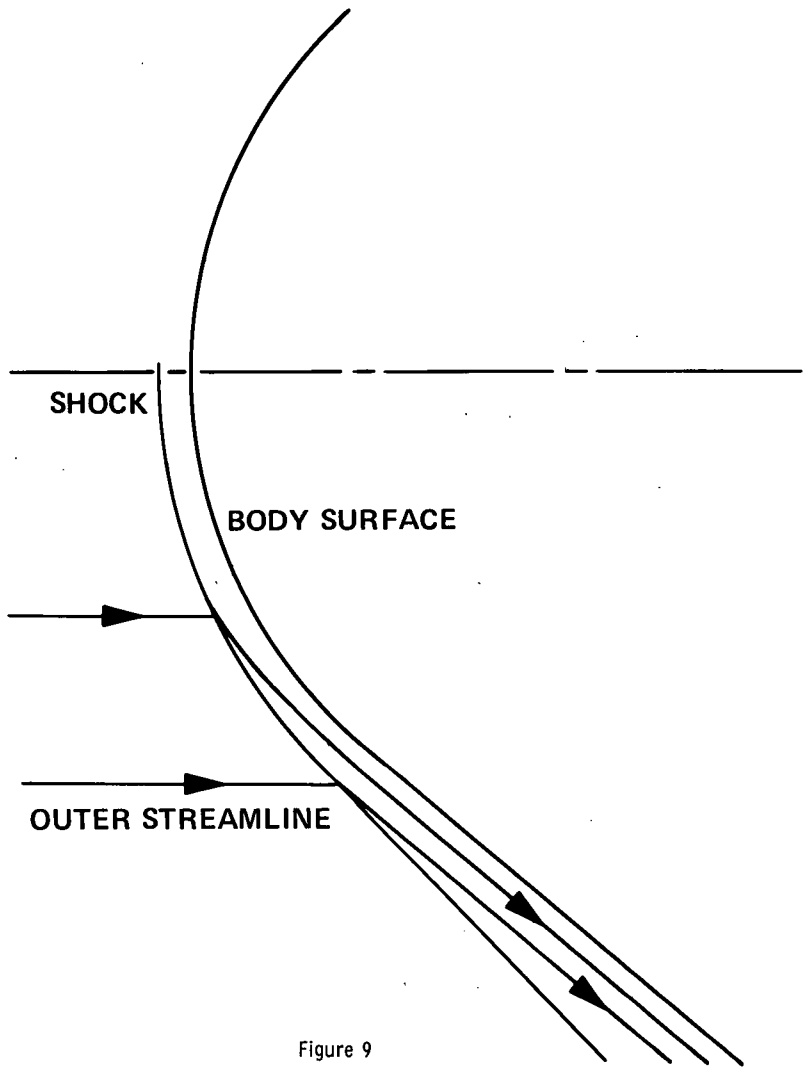

Figure 9

EQUILIBRIUM AND NONEQUILIBRIUM FLOW CALCULATIONS
(Fig. 10)

Calculations of the flow along selected streamlines have been made for both equilibrium and nonequilibrium chemical reactions. The trajectory points at which calculations were done are listed in the table below. Calculations have been made along the body surface streamline, a streamline about in the middle of the entropy layer and the outer streamline, or that which passes through the limiting oblique shock. The influence of changes in angle of attack and nose radius are also demonstrated.

The departure from chemical equilibrium are of a different type for those streamlines near the body than for the outer streamlines. In the entropy layer, that is along those streamlines near the body surface, the flow approaches chemical equilibrium in the stagnation region and then departs from equilibrium in the rapid expansion of the flow around the nose of the body. Along the outer streamlines, the flow is very much like the relaxing flow behind a shock wave. The flow is chemically frozen through the shock wave and then approaches equilibrium over the entire body length. Thus, near the body surface the departure from equilibrium is a lag in the rate of recombination as the flow expands from the stagnation point, while along the outer streamlines there is a lag in the dissociation rate.

TRAJECTORY POINTS USED IN STREAMLINE CALCULATIONS

1. V_∞ = 4.877 km/sec, h = 60.96 km (16 kfps) (200 kft)

2. V_∞ = 6.096 km/sec, h = 67.06 km (20 kfps) (220 kft)

3. V_∞ = 7.315 km/sec, h = 76.20 km (24 kfps) (250 kft)

Figure 10

FLOW ALONG BODY SURFACE STREAMLINES
(Fig. 11)

Several calculations have been made for the flow along the body surface streamline, starting from an equilibrium stagnation point. In the altitude range of 200 to 250 kft, the flow along the body surface streamlines is composed mainly of N_2, N, and O for both equilibrium and nonequilibrium flow. The principal nonequilibrium effect is the lag in the nitrogen atom recombination as the flow expands in the nose region. The oxygen is fully dissociated and remains so. The variation in temperature, density, velocity, and species concentrations along the streamline are illustrated in the figures below for the trajectory point V_∞ = 4.877 km/sec (16,000 fps), h = 60.96 km (200,000 ft), and for R_N = 1.22 m (4 ft), and $\alpha = 20°$.

The temperature distribution is a direct consequence of the nonequilibrium effect on the N-atom recombination rate. The nonequilibrium flow temperature falls much below the equilibrium temperature in the nose region because the nitrogen atom recombination reaction becomes frozen. Then, in the fairly uniform flow on the flat aftersurface, some recombination takes place and the nonequilibrium temperature approaches the equilibrium value toward the base of the body. Notice that this approach is gradual and the flow is almost frozen over the entire body. The nonequilibrium effects on density and velocity are slight and in the direction such that there is very little effect on the mass flow rate.

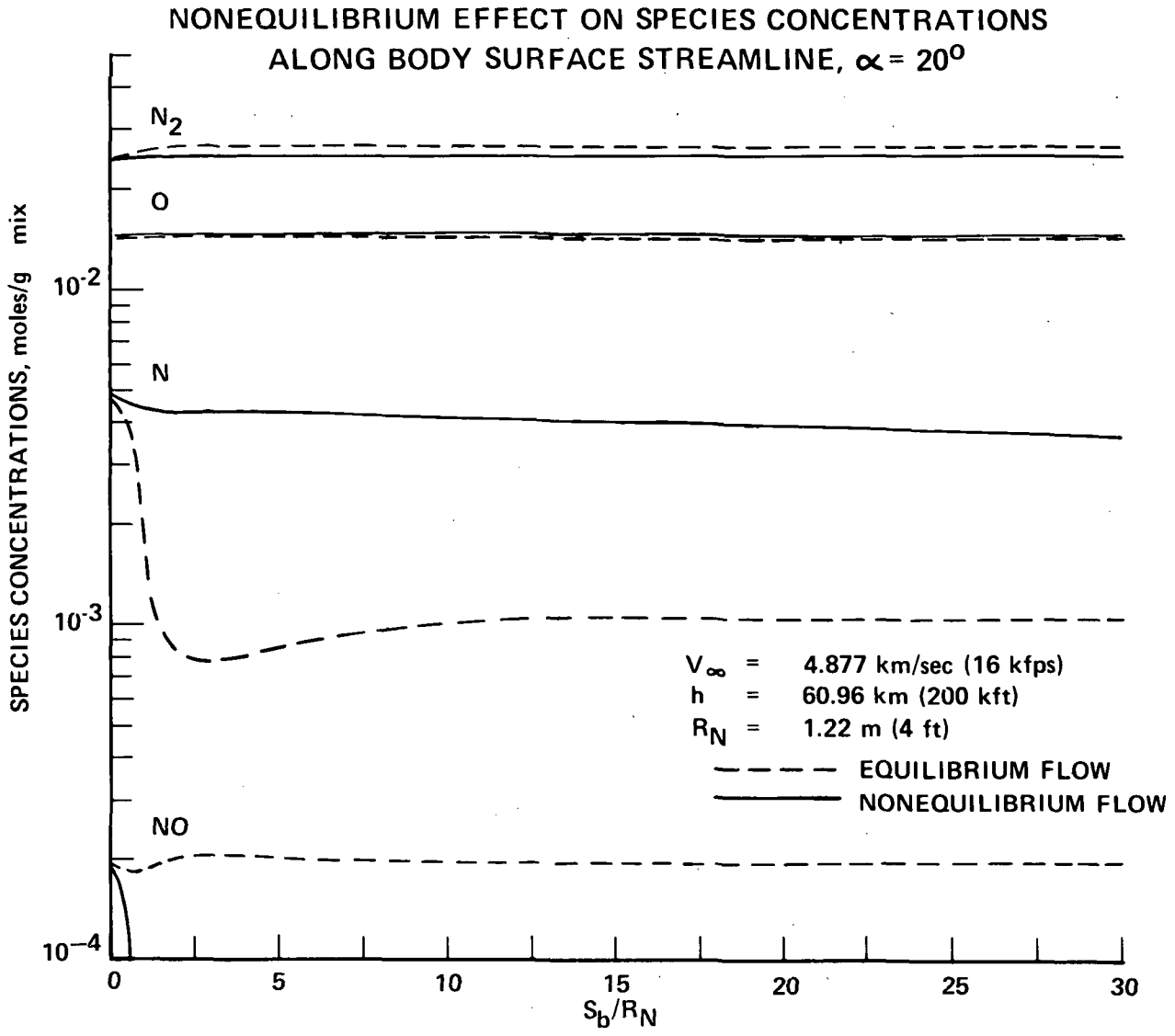
NONEQUILIBRIUM EFFECT ON SPECIES CONCENTRATIONS
ALONG BODY SURFACE STREAMLINE, α = 20°
SPECIES CONCENTRATIONS, moles/g mix
N2
O
N
NO
10-2
10-3
10-4
V∞ = 4.877 km/sec (16 kfps)
h = 60.96 km (200 kft)
RN = 1.22 m (4 ft)
EQUILIBRIUM FLOW
NONEQUILIBRIUM FLOW
0
5
10
15
20
25
30
Sb/RN

Figure 11(a)

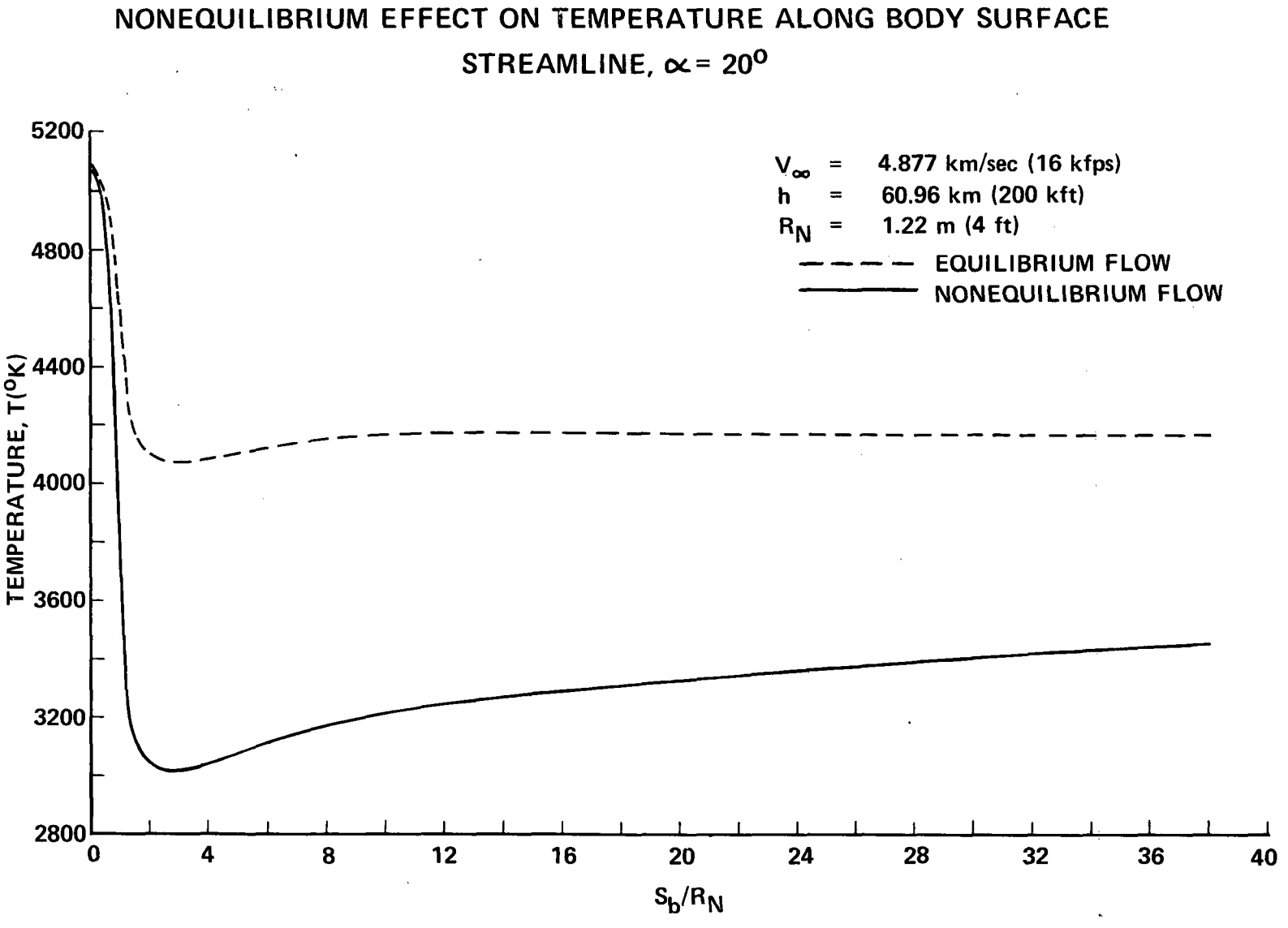
NONEQUILIBRIUM EFFECT ON TEMPERATURE ALONG BODY SURFACE
STREAMLINE, α = 20°
V_∞ = 4.877 km/sec (16 kfps)
h = 60.96 km (200 kft)
R_N = 1.22 m (4 ft)
EQUILIBRIUM FLOW
NONEQUILIBRIUM FLOW
TEMPERATURE, T(°K)
5200
4800
4400
4000
3600
3200
2800
0
4
8
12
16
20
24
28
32
36
40
S_b/R_N

Figure 11(b)

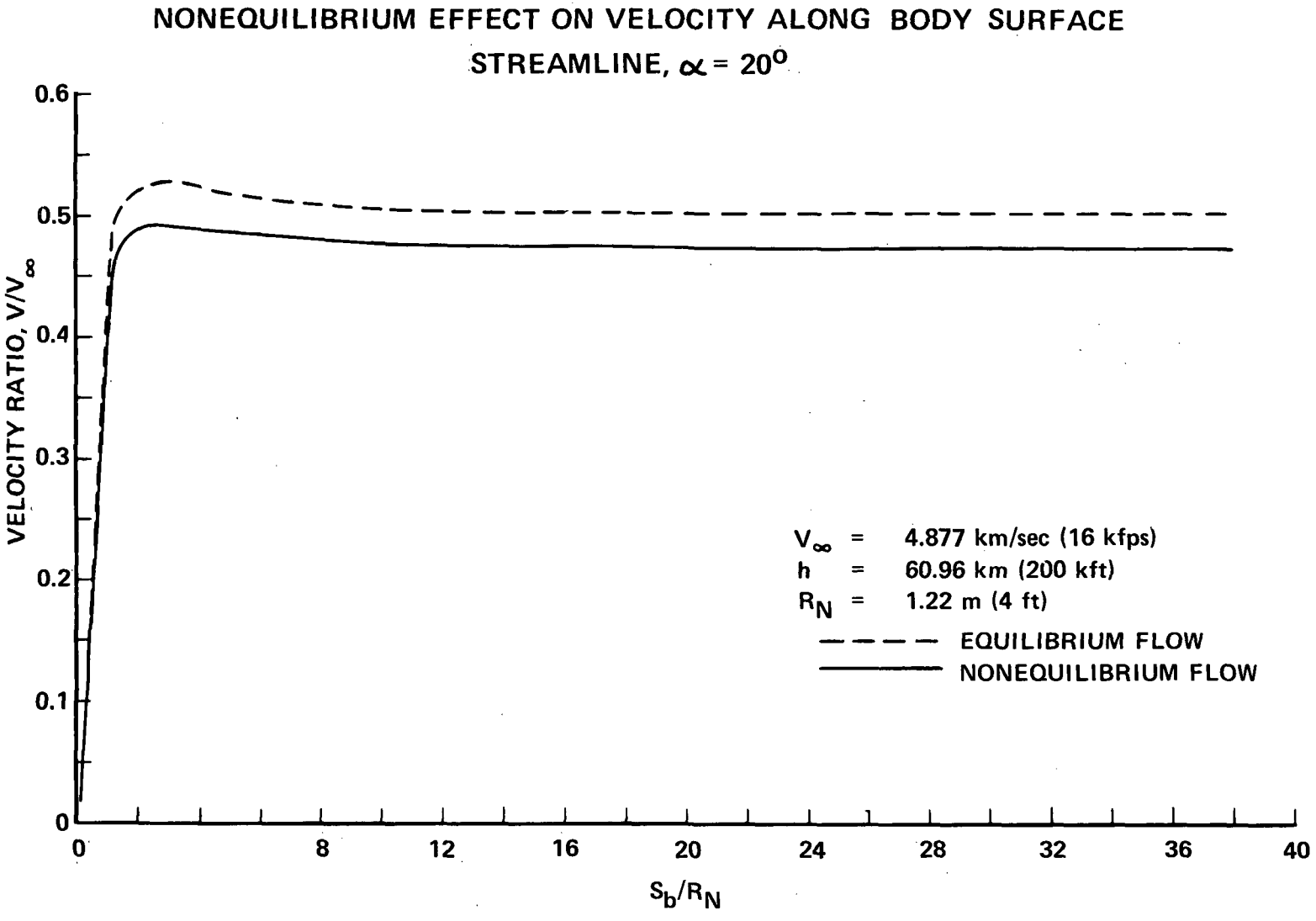
NONEQUILIBRIUM EFFECT ON VELOCITY ALONG BODY SURFACE STREAMLINE, α = 20°
VELOCITY RATIO, V/V∞
0.6
0.5
0.4
0.3
0.2
0.1
0
0
8
12
16
20
24
28
32
36
40
Sb/RN
V∞ = 4.877 km/sec (16 kfps)
h = 60.96 km (200 kft)
RN = 1.22 m (4 ft)
EQUILIBRIUM FLOW
NONEQUILIBRIUM FLOW

Figure 11(c)

Page intentionally left blank

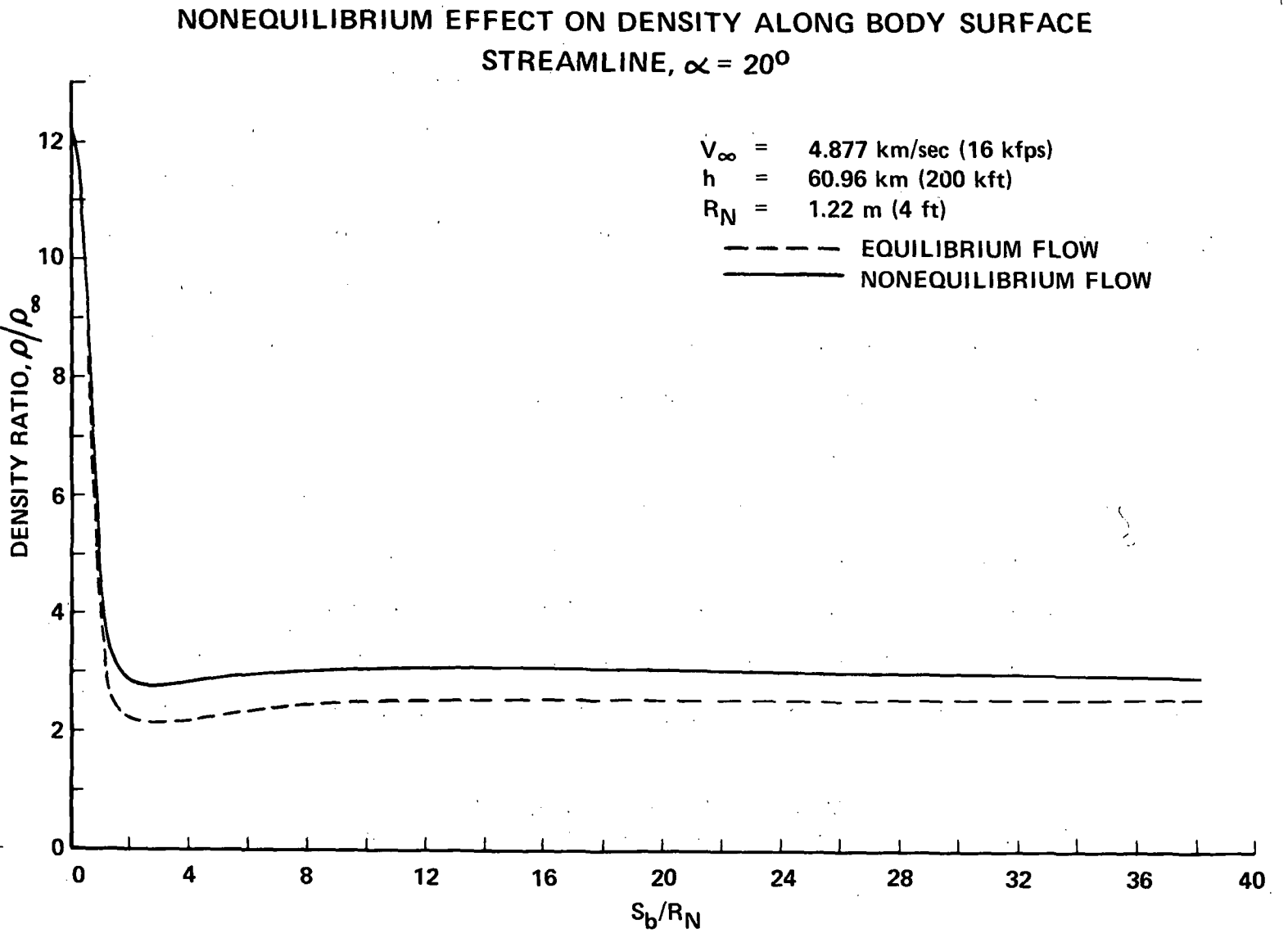
NONEQUILIBRIUM EFFECT ON DENSITY ALONG BODY SURFACE STREAMLINE, $\alpha = 20^o$
V_∞ = 4.877 km/sec (16 kfps)
h = 60.96 km (200 kft)
R_N = 1.22 m (4 ft)
EQUILIBRIUM FLOW
NONEQUILIBRIUM FLOW
DENSITY RATIO, ρ/ρ_∞
0
2
4
6
8
10
12
0
4
8
12
16
20
24
28
32
36
40
S_b/R_N

Figure 11(d)

TRAJECTORY VARIATION OF NONEQUILIBRIUM EFFECTS ON THE BODY STREAMLINE FLOW (Fig. 12)

Numerical solutions were obtained for the equilibrium and nonequilibrium flow along the body streamlines for the three trajectory points given in the table of Fig. 10. These calculations were done for an angle of attack of 20° and a body nose radius of 1.22 m (4 ft). The variation of the nonequilibrium effects from one trajectory point to the next is one of degree rather than kind. In this series of calculations, the temperature distributions are all similar to that shown in Fig. 11 and so the difference between the equilibrium and nonequilibrium flow temperatures at the base of the body is a good representation of the effect of nonequilibrium chemical reaction on the body streamline flow for these conditions. Accordingly, these temperatures are listed in the table for the three trajectory points at which calculations were made. The difference between the equilibrium and nonequilibrium temperatures is greatest at the highest altitude, highest velocity point because the nitrogen dissociation is greatest there and the most energy is frozen in chemical composition for this case.

NONEQUILIBRIUM EFFECTS ON SURFACE STREAMLINE TEMPERATURE

TRAJECTORY POINT	T_{EQ} (^{o}K)	T_{NEQ}* (^{o}K)
1. V = 4.877 km/sec (16 kfps) h = 60.96 km (200 kft)	4178	3459
2. V = 6.096 km/sec (20 kfps) h = 67.06 km (220 kft)	4973	3721
3. V = 7.315 km/sec (24 kfps) h = 76.20 km (250 kft)	5198	3372

* AT S_b = 45.6 m (150 ft)

Figure 12

FLOW ALONG OUTER STREAMLINES
(Fig. 13)

The flow along the outer streamlines in the blunted-delta wing flow field is much like the flow behind an oblique shock wave. The reacting flow behind strong shock waves was extensively reviewed in Ref. 7. There several calculations were made to investigate scaling and distances to equilibrium. In addition, the mapping of normal shock wave flows to approximate wedge flows was shown to be quite accurate. The results found here are very much in line with what would be expected in terms of the flow behind such equivalent normal shocks. At the velocities and altitudes of interest the distances to equilibrium can be considerable. For an angle of attack of 20°, the shock angle determined by the limiting pressure ratio is about 25° and varies little from one trajectory point to the next. The flow behind this wave, computed here as a constant pressure streamline flow, is essentially frozen over the length of the orbiter. The temperature at a distance of 45.6 m (150 ft) from the shock wave is shown for three trajectory points in the table below. At the lowest altitude of interest here, it can be seen that the flow is essentially an ideal gas flow. At the highest velocity and highest altitude, the difference between the equilibrium and non-equilibrium flow temperature is significant. Along the outer streamlines this discrepancy is due mainly to a lag in the oxygen dissociation rate and nitric oxide formation while the nitrogen remains virtually undissociated.

NONEQUILIBRIUM EFFECTS ON OUTER STREAMLINE TEMPERATURE

$\alpha = 20^o$ $R_N = 1.22$ m (4 ft)

TRAJECTORY POINT	T_{EQ} (^{o}K)	T_{NEQ}* (^{o}K)
1. V = 4.877 km/sec (16 kfps) h = 60.96 km (200 kft)	2053	2120
2. V = 6.096 km/sec (20 kfps) h = 67.06 km (220 kft)	2486	2997
3. V = 7.315 km/sec (24 kfps) h = 76.20 km (250 kft)	2707	3720

* AT S_b = 45.6 m (150 ft)

Figure 13

NONEQUILIBRIUM EFFECTS ON THE TEMPERATURE DISTRIBUTION THROUGH THE SHOCK LAYER (Fig. 14)

The manner in which chemical nonequilibrium effects change as attention is focused in turn on streamlines near the body surface and then on streamlines further out in the shock layer was briefly described in Fig. 10. Along the body streamline the static temperature of the nonequilibrium flow falls significantly below the equilibrium flow value as the flow expands around the nose. Along the outer streamlines, the temperature in the nonequilibrium flow increases toward the equilibrium value as the flow approaches chemical equilibrium. For one of the trajectory points, V_∞ = 4.877 km/sec (16,000 fps), h = 60.96 km (200,000 ft), α = 20°, the flow along several streamlines in the shock layer has been computed. The results for the variation of the temperature normal to the body surface are shown in this figure for S_b/R_N = 30, where S_b is the distance along the body from the stagnation point. The relative values for equilibrium and nonequilibrium flow reflect the behavior of the flow chemistry, as described above. For this case the flow along the streamlines outside the entropy layer is essentially an ideal gas flow.

NONEQUILIBRIUM EFFECT ON TEMPERATURE DISTRIBUTION THROUGH THE SHOCK LAYER

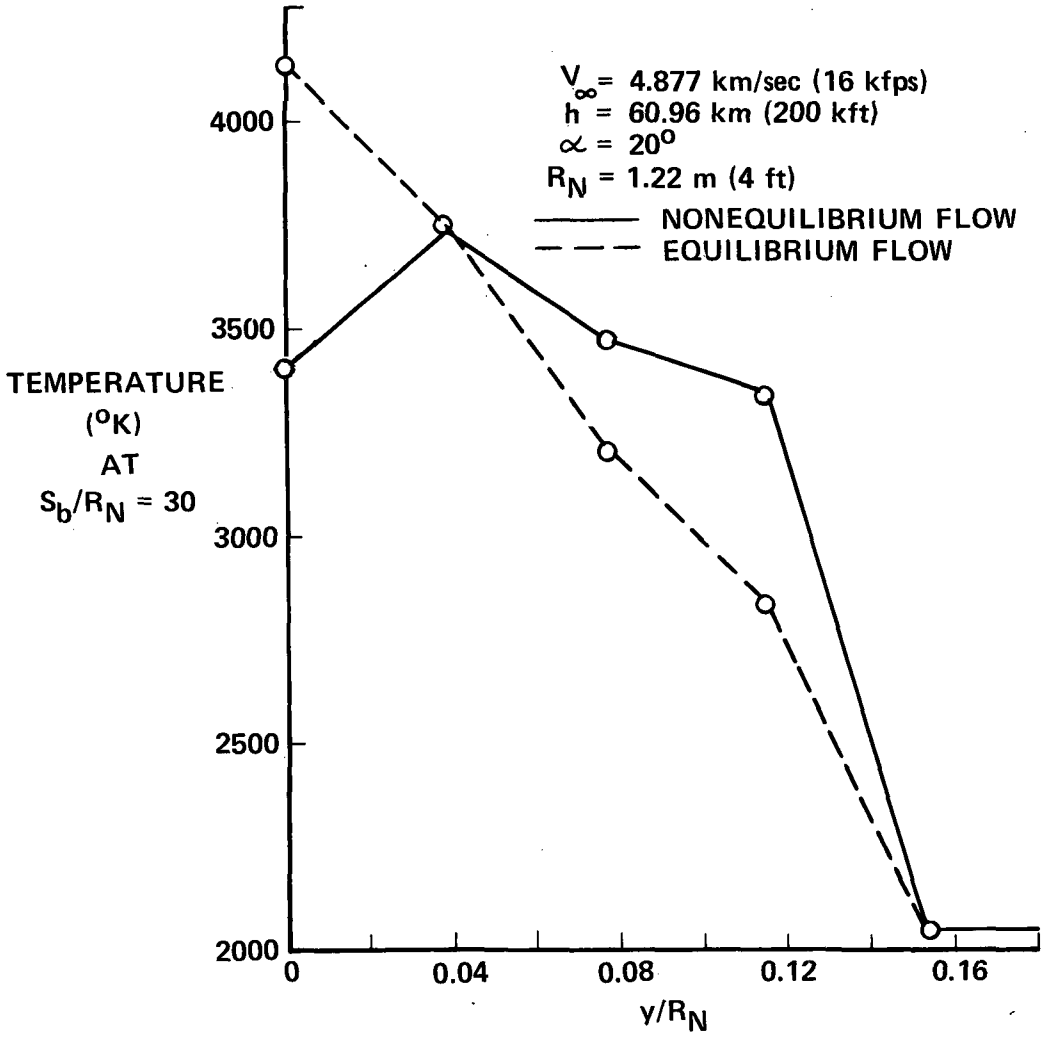

Figure 14

EFFECT OF ANGLE OF ATTACK
(Fig. 15 and 16)

Streamline calculations have also been made at $\alpha = 40°$. At this angle of attack the flow expansion around the nose of the body is weaker. Hence there is less of a lag in the recombination rate for nitrogen atoms. On the afterbody the density level is higher and the flow approaches equilibrium much more rapidly than for $\alpha = 20°$, both along the body streamlines and the outer streamlines. The temperature distribution along the body streamline and along the outermost streamline are illustrated below for the case $V_\infty = 4.877$ km/sec (16,000 fps), $h = 60.96$ km (200,000 ft), and $R_N = 1.22$ m (4 ft). Again these figures are typical of the results at the other trajectory points considered in this study.

NONEQUILIBRIUM EFFECT ON TEMPERATURE ALONG BODY SURFACE STREAMLINE, $\alpha = 40^{o}$

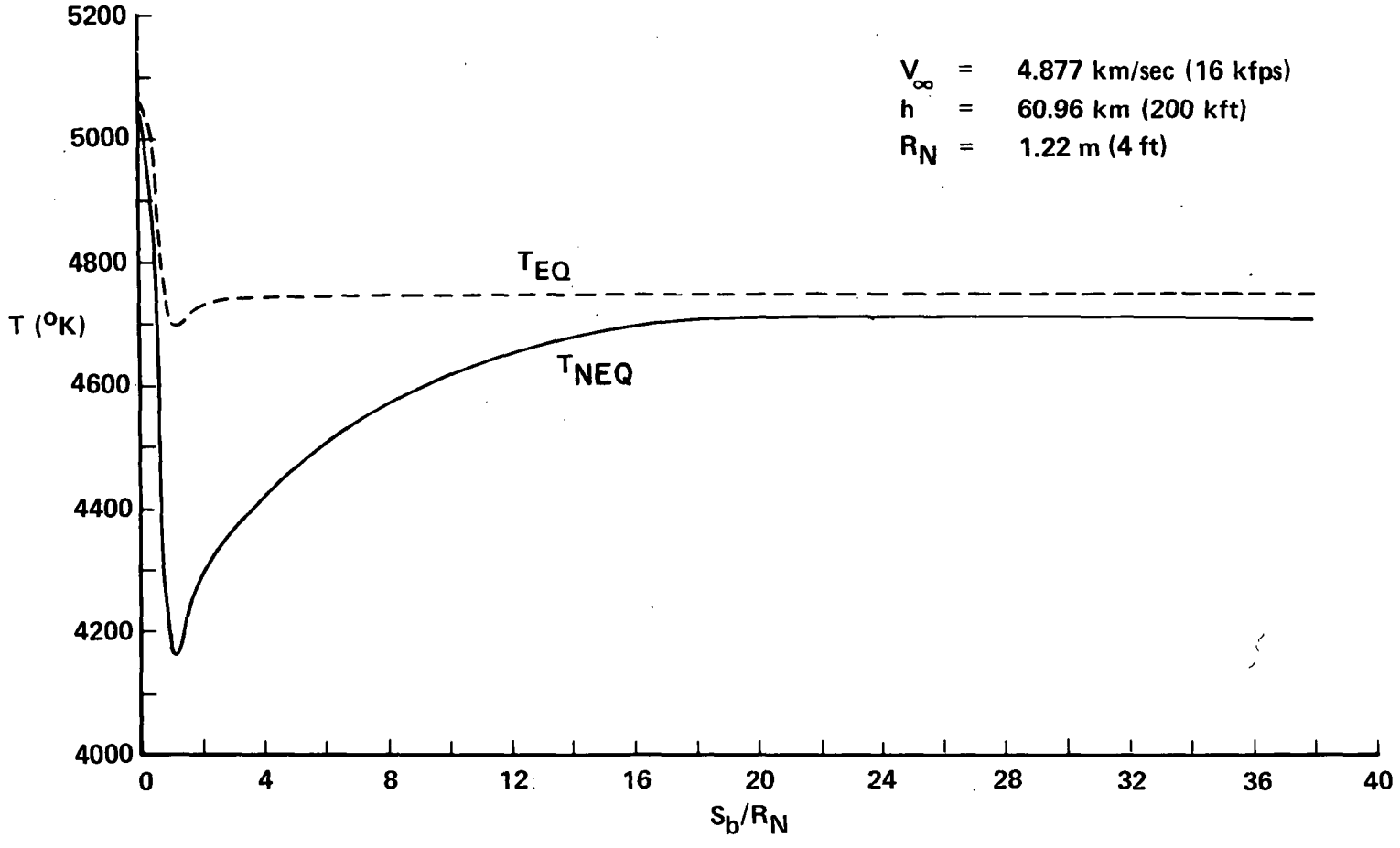

Figure 15

Page intentionally left blank

NONEQUILIBRIUM EFFECT ON TEMPERATURE ALONG OUTER STREAMLINE, $\alpha = 40^{o}$

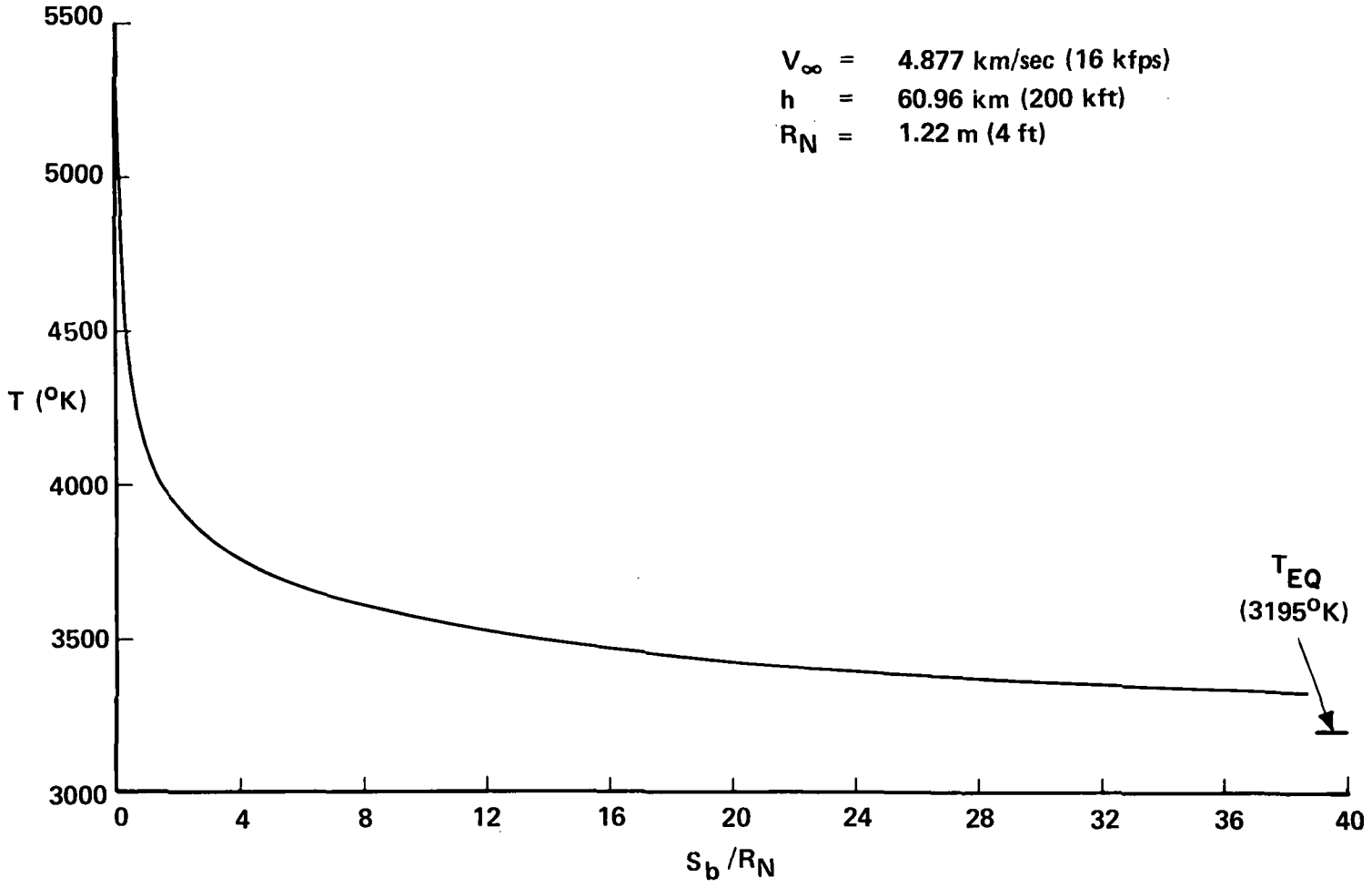

Figure 16

EFFECT OF NOSE RADIUS
(Fig. 17)

The flow along the outer streamlines is, of course, dependent only on the distance from the bow wave and is not influenced by the body nose radius. On the other hand, the flow along the streamlines in the entropy layer are affected by changes in body scale or nose bluntness. In the present framework, a change in body nose radius changes the rate at which the pressure drops in the expansion around the blunt nose. The rate of this pressure drop determines the departure from equilibrium. In order to investigate the effect of nose radius, the body streamline calculations for $\alpha = 20°$ were repeated for a body nose radius of .305 m (1 ft). Again the temperature variation along the streamline has been used to characterize the nonequilibrium effects. The equilibrium solution and the nonequilibrium solutions for $R_N = 0.305$ m (1 ft) and $R_N = 1.22$ m (4 ft) are compared in the accompanying figure. As indicated by these results very little more energy is frozen in the expansion around the smaller nose. In addition, the rate of increase toward equilibrium is about the same in terms of absolute distance, the temperatures being virtually identical at a distance of 45.7 m along the streamline. These results are typical for the range of trajectory points considered and nose radii in the .305 m to 1.22 m range. The flow along the body streamline becomes frozen in the expansion around the blunt nose and recombines only a slight amount over the body lengths of interest.

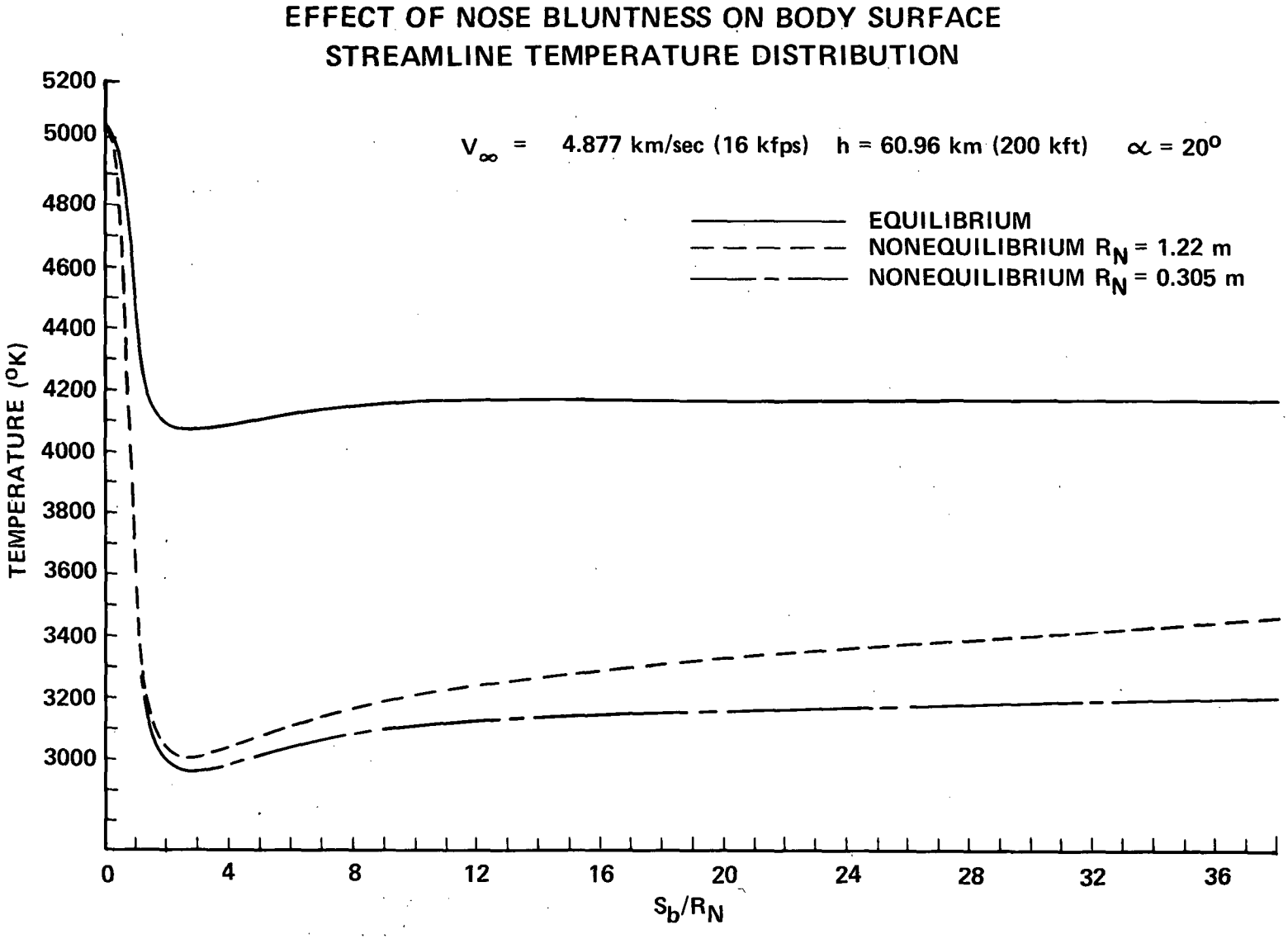
EFFECT OF NOSE BLUNTNESS ON BODY SURFACE
STREAMLINE TEMPERATURE DISTRIBUTION
V_∞ = 4.877 km/sec (16 kfps) h = 60.96 km (200 kft) $\alpha = 20^o$
EQUILIBRIUM
NONEQUILIBRIUM R_N = 1.22 m
NONEQUILIBRIUM R_N = 0.305 m
TEMPERATURE (^{o}K)
5200
5000
4800
4600
4400
4200
4000
3800
3600
3400
3200
3000
0
4
8
12
16
20
24
28
32
36
S_b/R_N

Figure 17

INFLUENCE OF CHEMICAL NONEQUILIBRIUM IN THE INVISCID FLOW FIELD ON SURFACE HEATING RATES
(Fig. 18)

The calculation of the inviscid flow on the shuttle orbiter influences estimates of the surface heating rates through the edge conditions used in the boundary layer calculations. For example, consider the laminar heat transfer rate in the nose region. For a chemically frozen boundary layer on a noncatalytic surface, a local similarity calculation gives the heat transfer rate proportional to $(H_{T_f} - h_w)$ where H_{T_f} is the total "frozen" enthalpy. Assuming that the body surface streamline is the edge streamline, the laminar heating rates for equilibrium and nonequilibrium flow in the body streamline are compared in the figure below. The results are shown for the case V_∞ = 7.32 km/sec (24,000 fps), h = 76.2 km (250,000 ft), α = 20°, R_N = 1.22 m (4 ft).

The assumption of frozen boundary layer flow was chosen as a point of comparison because the inviscid flow becomes frozen in the corner expansion and that indicates that the chemical state of the boundary layer will be far from equilibrium. It should also be noted that if the surface is completely catalytic the surface heat transfer rate depends very little on the chemical state of the boundary layer. Furthermore, the only way that nonequilibrium effects would then be important is through the transport properties.

In order to calculate accurately the influence of the inviscid flow on the surface heating rate the "swallowing" of the inviscid flow by the boundary layer should be accounted for. While this was not done in the above calculation, it is noted that calculations of the boundary layer thickness indicate that the boundary layer is thin compared to the shock layer. Thus, in the nose region the streamlines in the entropy layer, where nonequilibrium effects are most severe, determine the boundary layer edge conditions.

The entropy layer will be swallowed at some point along the body and the boundary layer edge conditions near the base of the body are determined by the outer streamlines of the inviscid flow. The ratio of $H_{T_f} - h_w$ for nonequilibrium flow to that for equilibrium flow along the outer streamlines is about 1.07 for the highest altitude, highest velocity case considered here. While the static temperatures are considerably different for the equilibrium and nonequilibrium flow along this streamline the frozen total enthalpy is not appreciably affected because the flow is a high Mach number flow and the static enthalpy is small compared to the total. Hence the nonequilibrium effects on the flow in the outer streamlines do not appear to have much of an effect on the surface heat transfer rate, at low angles of attack.

INFLUENCE OF NONEQUILIBRIUM INVISCID FLOWS ON THE LAMINAR HEATING RATE OF A FROZEN BOUNDARY LAYER ON A NONCATALYTIC SURFACE

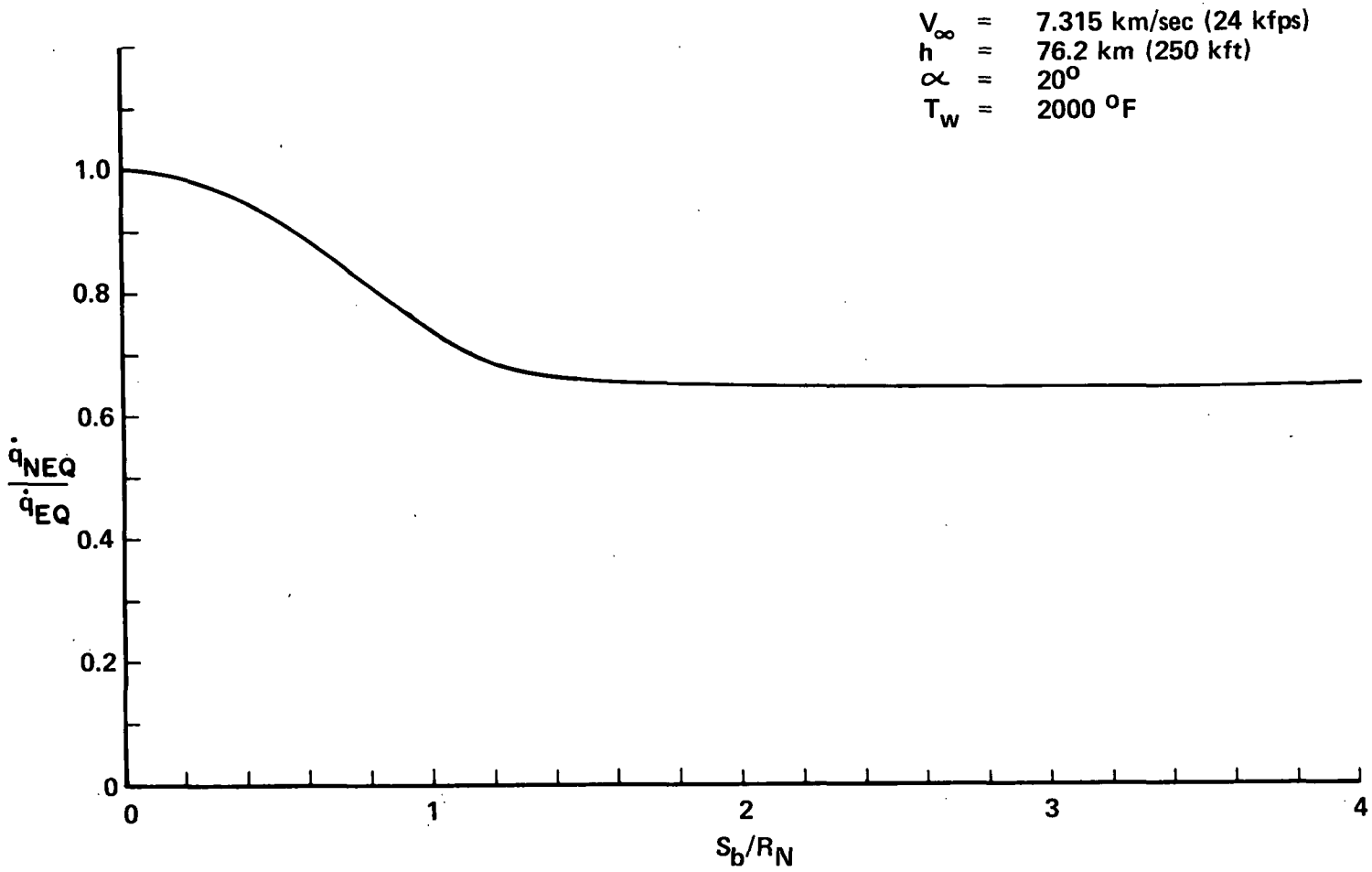

Figure 18

BOUNDARY LAYER THICKNESSES, TRANSITION, AND SWALLOWING OF THE ENTROPY LAYER
(Fig. 19)

The results of the inviscid streamtube computations have been applied to estimate boundary layer transition, the thicknesses of the laminar and turbulent boundary layers, and the location in the flow field where the entropy layer will be fully consumed by the boundary layer, i.e. entropy layer swallowing. Transition estimated were based on the NASA interim transition criterion. For $\alpha = 20°$, this criterion requires $R_{e_\theta}/M_e/(Re/\ell)^{1/5} \approx 10$, where all parameters are evaluated for conditions at the boundary layer edge. The laminar boundary layer thicknesses were estimated by using Cheng's two-dimensional local similarity solution,[8] generalized to relax the hypersonic approximations and to obtain a solution based on boundary layer edge conditions. For the present purposes, it was assumed that the boundary layer was fully turbulent immediately following transition, and the thickness estimates were based on the Spaulding-Chi theory[9] and on procedures given by Johnson.[10] The Spaulding-Chi theory was approximated by a logarithmic law, $F_c C_f \approx .039 \left[F_{R_x} \; Re_x\right]^{-1/6}$, with errors of less than 10%, and this was applied in the usual momentum integral relation for boundary layer thickness. The exponent in the power law velocity profile was determined from Johnson's relations, with an effective starting length defined to yield an approximate Blasius profile at transition. Transition and the boundary layer thicknesses were determined by using the various nonequilibrium streamlines in the entropy layer for edge conditions, and by using an equilibrium streamline processed by the oblique shock wave. The latter is often used in calculating boundary layer characteristics, and the present comparison provides a check on the accuracy of this procedure.

The results of these calculations are shown in Fig. 19 for the three trajectory points considered here and for an angle of attack of 20°. At an altitude of 61 km (200kft), Fig. 19(a), the calculations show that the laminar boundary layer thickness is insensitive to the edge conditions, but transition is strongly influenced. The streamlines are labeled according to their distance from the body surface. The transition location varies by a factor of 2 1/2, depending on whether the nonequilibrium body streamline or the equilibrium oblique shock streamline is used. For these flight conditions, the latter corresponds to an ideal gas streamline, and there are essentially no nonequilibrium effects in that portion of the flow field. The thickness of the entropy layer is indicated in the figure, and it shows that the laminar boundary layer and transition are governed by conditions in the nonequilibrium entropy layer. The predominate nonequilibrium effect in this region is in the static temperature, and it differs from the equilibrium value by about 30%. This enters directly into the criterion for transition length through the square of the Mach number.

It can be seen in Fig. 19(a) that following transition, the boundary layer thickens rapidly, and it is thicker by a factor of 2 where the nonequilibrium entropy layer governs the flow. These boundary layer estimates indicate that the nonequilibrium entropy layer is fully consumed in the boundary layer at a distance of about 20 nose radii from the leading edge, i.e. the boundary layer development on the forward half of the body is governed by the nonequilibrium entropy layer and the boundary layer on only the aft can be estimated using conditions based on the oblique shock wave.

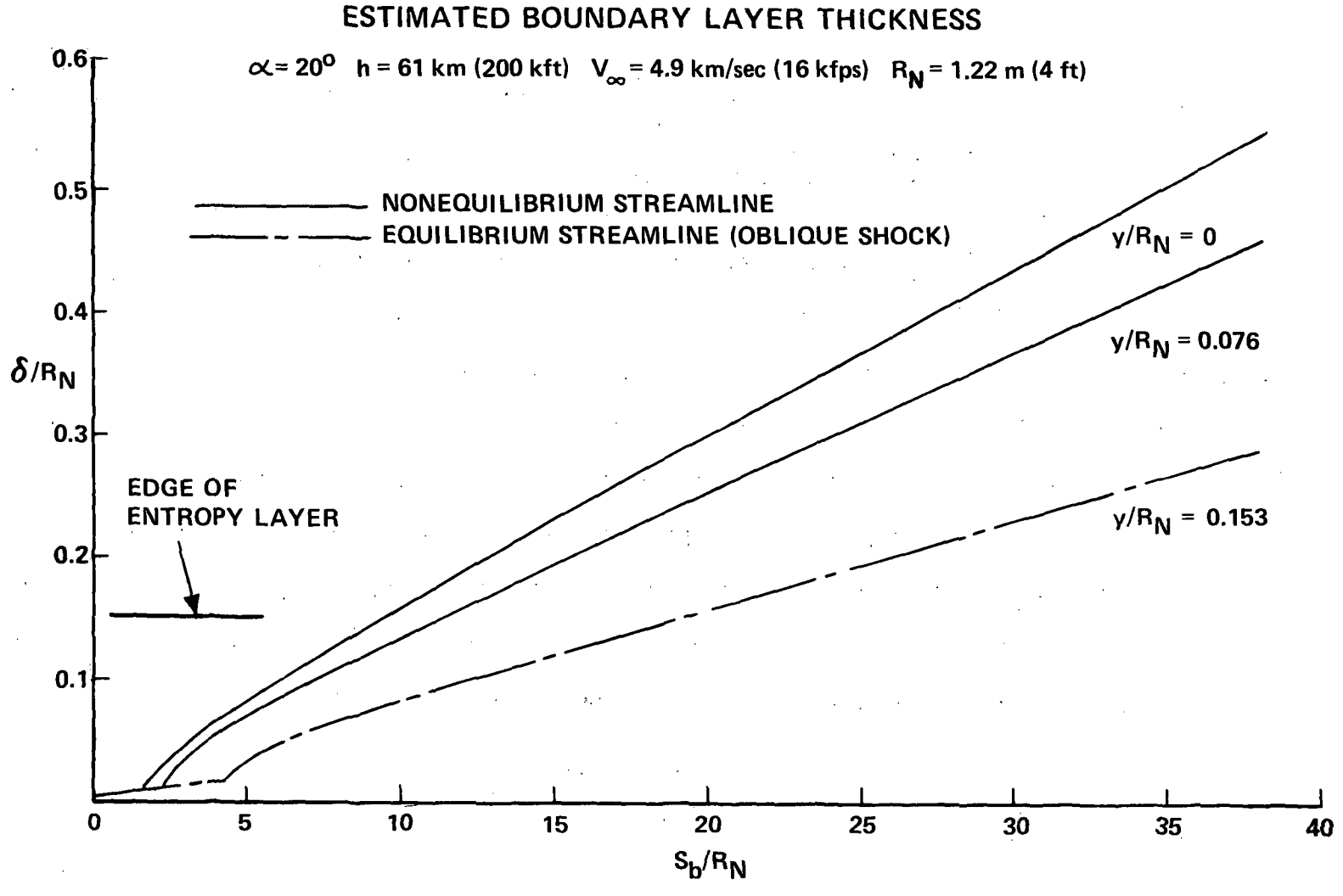
ESTIMATED BOUNDARY LAYER THICKNESS
α = 20° h = 61 km (200 kft) V∞ = 4.9 km/sec (16 kfps) RN = 1.22 m (4 ft)
NONEQUILIBRIUM STREAMLINE
EQUILIBRIUM STREAMLINE (OBLIQUE SHOCK)
y/RN = 0
y/RN = 0.076
y/RN = 0.153
EDGE OF ENTROPY LAYER
δ/RN
Sb/RN
0.6
0.5
0.4
0.3
0.2
0.1
0
5
10
15
20
25
30
35
40

Figure 19(a)

(Fig. 19(b))

The calculated boundary layer characteristics at an altitude of 67 km (220 kft) are shown in Fig. 19b. These show that the thickness of the laminar layer is influenced by the edge conditions, and that the laminar layer develops under conditions corresponding approximately to the nonequilibrium body streamline. Again these results show that the transition length is a factor of four shorter than that predicted using equilibrium oblique shock conditions. The thickness of the nonequilibrium entropy layer is shown in Fig. 19b, and it can be seen that much of the boundary layer develops under the influence of the entropy layer. For this flight condition, the nonequilibrium entropy layer is fully consumed by the boundary layer about sixteen nose radii from the leading edge. Consequently, nominally the forward half of the boundary layer is governed by nonequilibrium conditions in the entropy layer while the aft half is governed by equilibrium, or in this case, ideal gas conditions behind the oblique shock wave.

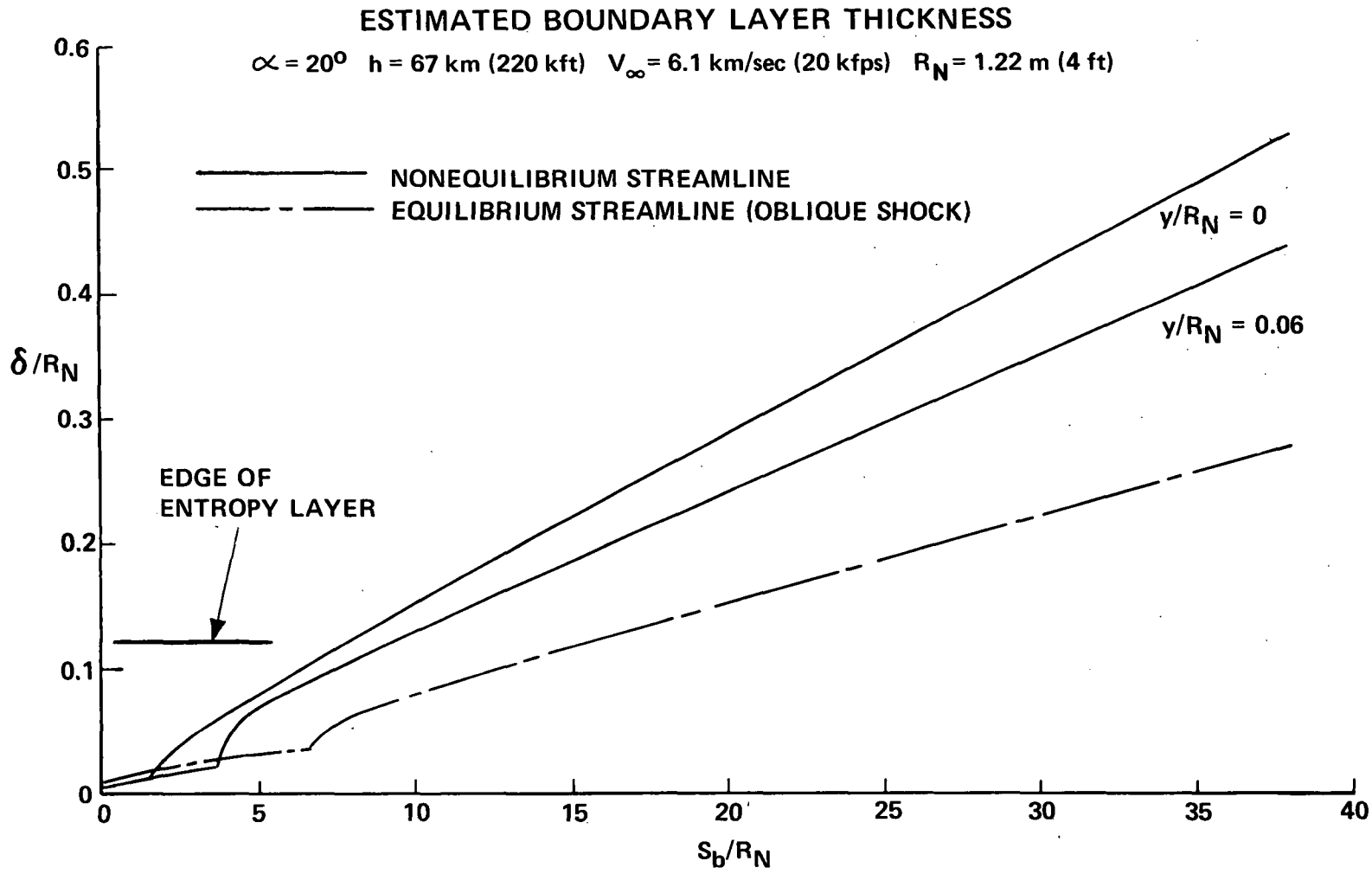
ESTIMATED BOUNDARY LAYER THICKNESS
$\alpha = 20^o$ h = 67 km (220 kft) V_∞ = 6.1 km/sec (20 kfps) R_N = 1.22 m (4 ft)
NONEQUILIBRIUM STREAMLINE
EQUILIBRIUM STREAMLINE (OBLIQUE SHOCK)
$y/R_N = 0$
$y/R_N = 0.06$
EDGE OF ENTROPY LAYER
δ/R_N
S_b/R_N
0.6
0.5
0.4
0.3
0.2
0.1
0
0
5
10
15
20
25
30
35
40

Figure 19(b)

(Fig. 19(c))

The calculated boundary layer characteristics at an altitude of 76 km (250 kft) are shown in Fig. 19c. These show that the thickness of the laminar layer is influenced appreciably by the assumed edge conditions, differing by a factor of two for the streamlines considered. Again, transition is strongly and adversely effected by the nonequilibrium entropy layer and is predicted to occur at $S_b / R_N = 5$ as compared with the prediction based on the equilibrium oblique shock conditions at $S_b / R_N = 17$. For this flight condition, the entire inviscid flow field is affected by thermochemical nonequilibrium and it is not appropriate to calculate streamline conditions based on equilibrium flow behind the oblique shock. The streamline at $y / R_N = 0.1$ is processed by the oblique wave, and the nonequilibrium effects on boundary layer thickness can be seen by comparing the results for that streamline with those for the equilibrium oblique shock streamline. The entropy layer is thinner that at the lower altitudes and the indications are that it will be consumed by the boundary layer at about 12 to 14 nose radii from the leading edge. For this case, about 1/3 of the body length is dominated by the nonequilibrium entropy layer, and the entire inviscid flow field is influenced by nonequilibrium effects.

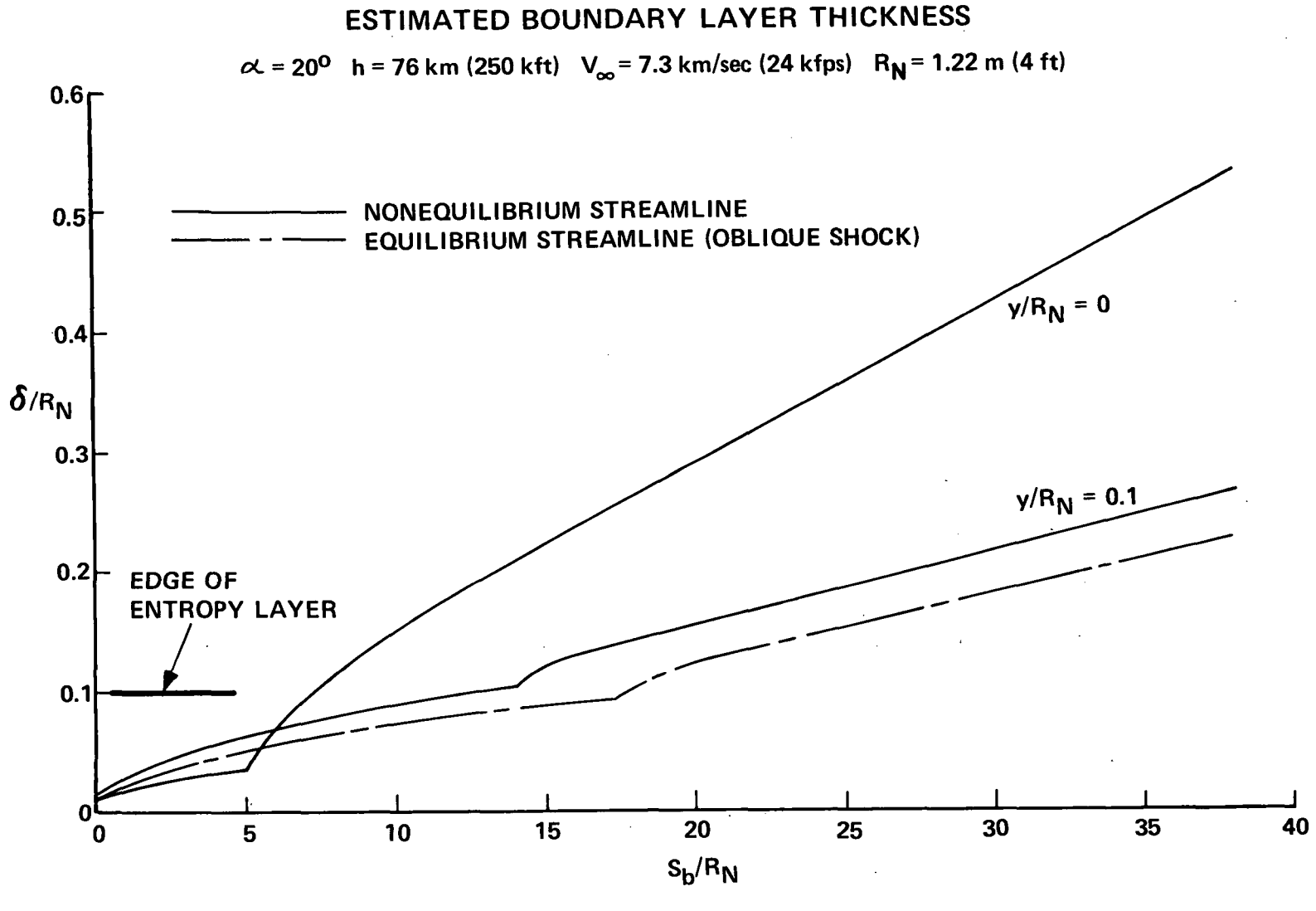
ESTIMATED BOUNDARY LAYER THICKNESS
α = 20° h = 76 km (250 kft) V∞ = 7.3 km/sec (24 kfps) RN = 1.22 m (4 ft)
NONEQUILIBRIUM STREAMLINE
EQUILIBRIUM STREAMLINE (OBLIQUE SHOCK)
y/RN = 0
y/RN = 0.1
EDGE OF ENTROPY LAYER
δ/RN
Sb/RN
0.6
0.5
0.4
0.3
0.2
0.1
0
0
5
10
15
20
25
30
35
40

Figure 19(c)

SUMMARY

The degree of chemical nonequilibrium in the inviscid flow field of a blunted delta body typical of a shuttle orbiter was examined. This investigation was carried out within the framework of numerical calculations of the reacting flow along selected streamlines in the windward plane of symmetry. An approximate model of the pressure field was devised and the reacting streamline flows were computed for specified pressure histories.

Pressure data obtained on two test shapes, a blunted delta wing and a straight-wing body were presented. Experimental results were presented at angles of attack of 0, 20°, 40°, and 60°. Streamline calculations were performed at three typical trajectory points in the altitude range of 60.96 to 76.2 km (200 to 250 kft). Results were obtained for two angles of attack, 20° and 40°, and for two nose radii, 0.305 m and 1.22 m (1 ft and 4 ft).

Most of the calculations were done for the 20° angle of attack and the 1.22 m nose radius. The results for these cases were very similar over the range of trajectory points considered. On the streamlines close to the body the flow approaches chemical equilibrium in the stagnation region and then freezes in the expansion around the spherical nose. Along the inner streamlines the flow is composed of essentially N_2, N, and O for the conditions treated. Along the outer streamlines, the flow was essentially frozen for the 20° angle of attack. The difference between the equilibrium and nonequilibrium solutions became appreciable at the highest trajectory point considered.

The effect of angle of attack was investigated by computing streamline flows for $\alpha = 40°$ and comparing them with the $\alpha = 20°$ results. The increase in density level on the windward surface was sufficient to promote an approach to chemical equilibrium along both the inner and outer streamlines in the shock layer. The calculations carried out for $R_N = 0.305$ m (1 ft) indicated very little effect of nose radius or scale on the degree of nonequilibrium. This is because the flow along the body streamline freezes even for larger values of the nose radius. The streamline outside the entropy layer are independent of nose bluntness effects.

The edge conditions of the laminar boundary layer in the nose region are determined by streamlines which pass through the nearly normal portion of the bow shock. On the other hand the streamlines which pass through the limiting oblique shock determine the edge conditions of the boundary layer toward the base of the body. The calculations done here for an angle of attack of 20° show a fairly large fraction of the total enthalpy, e.g. about 30%, can be frozen in the chemistry along the body streamlines. On the other hand, in the flow along the outer streamlines the chemistry is nearly frozen but accounts for less than 10% of the total enthalpy. As the angle of attack increases the fraction of the total enthalpy accounted for by dissociation increases, but so does the rate of dissociation. At an angle of attack of 40°, the flow in the outer streamlines is near equilibrium over most of the length of the vehicle.

The influence of nonequilibrium effects on the boundary layer has been estimated using approximate boundary layer calculations. These show that for all three trajectory points, the laminar boundary layer development is governed by the nonequilibrium entropy layer. In each case, transition is determined by conditions in the nonequilibrium entropy layer and not by conditions behind the oblique wave. In each case the effect was detrimental in that transition occurred substantially earlier than predicted on the basis of equilibrium flow behind the oblique shock. In all cases covered, the nonequilibrium entropy layer governs the boundary layer development on the forward 1/3 to 1/2 of the body. The boundary layer development on the aft portions is governed by equilibrium flow behind the oblique shock at the two lower altitudes, and by nonequilibrium flow behind the oblique shock wave at the highest altitude.

There are several features of the nonequilibrium flow over a shuttle orbiter which deserve mention before concluding. First, it should be noted that the flow in the windward plane of symmetry does not necessarily represent the extreme so far as chemical nonequilibrium effects are concerned. Along streamlines which enter the nearly normal portion of the bow shock on the windward side but are then swept around the edge of the body to the leeward side, the flow undergoes a much greater expansion than in the plane of symmetry. Consequently, the difference between the equilibrium and nonequilibrium flow

properties and composition along such streamlines could be greater than along those treated in this study.

Although the presence of ionization was allowed for in the calculations the results for the electron concentration have not been presented in detail. However, the effect of nonequilibrium in the ionization and deionization reactions is even more pronounced than on the neutral chemistry. For the range of conditions considered here the electron number densities were between 10^{13} cc^{-1} and 10^{14} cc^{-1} in the nose region and between 10^{11} cc^{-1} and 10^{12} cc^{-1} at the base of the body.

The results of the present study indicate that nonequilibrium effects will persist at altitudes below 60.96 km (200,000 ft) for those streamlines near the body surface. Also nonequilibrium effects along the outer streamlines could be important at higher angles of attack at altitudes above 76.2 km (250,000 ft).

For the range of trajectory points considered here the nonequilibrium effects on a blunted delta shape at an angle of attack of 20^{o} are much like those in the flow on blunted slender cones. Nonequilibrium effects are most important in the entropy layer. However, significant effects on the temperature and composition exist throughout the flow field in portions of the orbiter entry trajectory. The influence of the nonequilibrium effects on the boundary-layer edge conditions have been discussed. However, the nonequilibrium effects on the viscous portions of the flow field have not been treated beyond this. Furthermore the results of the present work indicate that the flow in the boundary layer will be far from equilibrium in the altitude range above 60.96 km (200,000 ft).

REFERENCES

1. Wittliff, C.E.; and Sundaram, T.R.: A Study of Real-Gas Effects on Blunted Cone Flows. AEDC-TR-69-36, 1969.

2. Schaefer, W.T. Jr.: Characteristics of Major Active Wind Tunnels at the Langley Research Center. NASA TMX-1130, 1965.

3. Lordi, J.A.; Mates, R.E.; and Moselle, J.R.: Computer Program for the Numerical Solution of Nonequilibrium Expansions of Reacting Gas Mixtures. NASA CR-472, 1966.

4. Inouye, M.: Shock Standoff Distance for Equilibrium Flow Around Hemispheres Obtained from Numerical Calculations. AIAA J. Vol. 3, No. 1, Jan. 1965, p. 172.

5. Wittliff, C.E.; and Curtis, J.T.: Normal Shock Wave Parameters in Equilibrium Air. Cornell Aeronautical Laboratory Report No. CAL-111, 1961.

6. Thomas, P.D.; Vinokur, M.; Bastianon, R.; and Conti, R.J.: Numerical Solutions for the Three Dimensional Hypersonic Flow Field of a Blunt Delta Body. AIAA Paper 71-596, AIAA 4th Fluid and Plasma Dynamics Conference, Palo Alto, Calif. June 21-23, 1971.

7. Wittliff, C.E.; Sundaram, T.R.; Rae, W.J.; and Lordi, J.A.: A Study of High-Density Hypervelocity Flows and Similitudes. AEDC-TR-67-72, 1967.

8. Cheng, H.K.; Hall, J.G.; Golian, T.C.; and Hertzberg, A.: Boundary Layer Displacement and Leading-Edge Bluntness Effects in High Temperature Hypersonic Flow. JAS, Vol. 28, No. 5, May 1961, p. 353.

9. Spaulding, D.B. and Chi, S.W.: The Drag of Compressible Turbulent Boundary Layer on a Smooth Flat Plate With and Without Heat Transfer. J.F.M., Vol. 18, Pt. 1, Jan. 1964, p. 117.

10. Johnson, C.B. and Boney, L.R.: A Simple Method for the Calculation of Real-Gas Turbulent Boundary Layers with Variable Edge Entropy. NASA TN D-6217, June 1971.